Triangular and Ramp Waveforms in Target Detection with a Frequency Modulated Continuous Wave Radar

Pasi Koivumäki

School of Electrical Engineering

Thesis submitted for examination for the degree of Master of Science in Technology.

Espoo 23/01/2017

Thesis supervisor:

Prof. Keijo Nikoskinen

Thesis advisor:

D.Sc. (Tech.) Tero Kiuru

Aalto University
School of Electrical
Engineering

AALTO UNIVERSITY
SCHOOL OF ELECTRICAL ENGINEERING

ABSTRACT OF THE
MASTER'S THESIS

Author: Pasi Koivumäki

Title: Triangular and Ramp Waveforms in Target Detection with a Frequency Modulated Continuous Wave Radar

Date: 23/01/2017 Language: English Number of pages: 7+77

Department of Radio Science and Technology

Professorship: Radio Science and Engineering

Supervisor: Prof. Keijo Nikoskinen

Advisor: D.Sc. (Tech.) Tero Kiuru

The goal of this thesis was to study how a triangular chirp can be used in target detection and parameter estimation with an FMCW radar. The history of radar technology is briefly discussed, and motivation for the research is presented with a review of some FMCW radar applications. The triangular chirp is compared with slow-time processed ramp chirps on a theoretical basis. A method of improving the accuracy of triangular chirps with zero padding is presented. The process of zero padding is demonstrated with a MATLAB example, and then applied to real measurement data.

The measurements were performed in an anechoic chamber and an office environment. Range and radial velocity of a single target were considered. A walking person was used as the test target. A highly accurate laser sensor was used as a reference.

The results demonstrate that the accuracy of a triangular chirp can be greatly improved with zero padding, which allows much shorter chirps to be used while maintaining a high accuracy. For example, a zero padded 1000 µs long triangular chirp was used to determine the radial velocity of a walking target with an accuracy of approximately 0.25 m/s. In comparison, without zero padding the accuracy was approximately 2 m/s. To reach a comparable accuracy without zero padding, the triangular chirp would have to be significantly longer. At the end of the thesis, topics for further research are proposed.

Keywords: FMCW, zero padding, resolution, accuracy, range, radial velocity

AALTO-YLIOPISTO
SÄHKÖTEKNIIKAN KORKEAKOULU

DIPLOMITYÖN
TIIVISTELMÄ

Tekijä: Pasi Koivumäki

Työn nimi: Kolmio- ja ramppiaallot kohteen havaitsemisessa taajuusmoduloidulla kantoaaltotutkalla

Päivämäärä: 23/01/2017 Kieli: Englanti Sivumäärä: 7+77

Radiotieteen ja -tekniikan laitos

Professuuri: Radiotiede ja -tekniikka

Työn valvoja: Prof. Keijo Nikoskinen

Työn ohjaaja: TkT Tero Kiuru

Työssä tutkitaan kuinka kolmioaaltoa voidaan käyttää havaitun kohteen paikan ja nopeuden määrittämiseen FMCW-tutkalla. Käsittelen alussa lyhyesti tutkien historiaa, ja FMCW-tutkien yleisiä sovelluksia. Kolmioaaltoa verrataan ramppiaaltoon teoreettiselta pohjalta. Esittelen työssä menetelmän kolmioaallon mittaustarkkuuden parantamiseksi lisäämällä näytteistettyyn signaaliin nollia. Menetelmää demonstroidaan MATLAB:illa ja lopulta sovelletaan mitattuun dataan.

Mittaukset suoritettiin radiokaiuttomassa huoneessa ja toimistotilassa. Tilaisuuksissa pyrittiin mittaamaan yksittäisen kohteen sijaintia ja liikenopeutta. Mittauskohteena toimi kävelevä ihminen. Mittausten vertailukohteena toimi lasersensori.

Saadut tulokset demonstroivat kolmioaallon tarkkuuden olevan merkittävästi parannettavissa esitetyllä menetelmällä. Korkean tarkkuuden säilyttäminen on mahdollista lyhyelläkin kolmioaallolla, joka ilman nollien lisäämistä olisi erittäin epätarkka. Esimerkiksi kävelevän kohteen nopeus mitattiin 1000 µs pituisella kolmioaallolla ja nollien lisäämisellä noin 0.25 m/s tarkkuudella, kun taas ilman nollia tarkkuus oli noin 2 m/s. Ilman nollien lisäystä kolmioaallon pituuden olisi oltava moninkertainen vastaavan tarkkuuden saavuttamiseksi. Työn lopussa esitetään aiheita jatkotutkimukselle.

Avainsanat: FMCW-tutka, mittausresoluutio, mittaustarkkuus, kohteen etäisyys, kohteen nopeus

Preface

I want to thank my instructor Tero Kiuru for his guidance and patience during the process of writing this thesis. Other VTT staff that played instrumental roles in completion of this thesis include Ismo Huhtinen, Mervi Hirvonen, and Mikko Metso. In addition I am grateful to my supervisor Keijo Nikoskinen for his positive attitude and faith in my abilities. In hindsight I can only say I wish I would have relied on these people more. Finally I wish to extend my gratitude to Jardak Seifallah for his work on programming the radar device used in this thesis and helping me get acquainted with it.

Otaniemi,

Pasi J. V. Koivumäki

Contents

Symbols and abbreviations

Symbols

B	bandwidth
c	speed of light in vacuum $\approx 3 \times 10^8$ [m/s]
ΔR	range resolution
ΔV	radial velocity resolution
f_b	beat frequency
$f_{b,\text{up}}$	ramp up section beat frequency of a triangular chirp
$f_{b,\text{down}}$	ramp down section beat frequency of a triangular chirp
f_c	carrier frequency
f_d	Doppler frequency
f_m	frequency shift due to sweep number
m	sweep number
M	total sweep number
N	number of samples
π	pi ≈ 3.14159264
R	range
R_{max}	maximum detectable range
R_{min}	mainimum detectable range
t_d	round-trip delay
T	chirp duration
T_s	sampling interval
V	radial velocity
V_{max}	maximum detectable radial velocity
V_{min}	minimum detectable radial velocity
u_{Tx}	transmitted signal
u_{Rx}	received signal
u_m	mix of transmitted and received signals

Abbreviations

CW	continuous wave
CRI	chirp repetition interval
DAC	digital analog converter
DDS	direct digital synthesizer
FFT	Fast Fourier Transform
FMCW	frequency modulated continuous wave
I/Q data	in-phase and quadrature data
LUT	look up table
PRI	pulse repetition interval
Rx	receiver
SNR	signal-to-noise ratio
Tx	transmitter

1 Introduction

1.1 Briefly on history of radars

Radars are electromagnetic devices used for detection of objects that reflect the signal transmitted by the radar. Essentially, they perform echolocation by means of electromagnetic radiation. A radar device transmits a signal that is reflected back to the device. The reflection can be analyzed to gain information about distance to a particular source of reflection, and other parameters. [1]

As it has been for many other technologies, the advent and development of radar systems was first fueled by military demand. The effects of World War II on radar technology in the United States are well documented [2, 3]. War was a driving force in the Soviet Union [4] and Japan [5] as well. Most of the techniques used in modern radar systems were developed for use in World War II, or soon after [6]. However, rapidly industrializing world of the time also had a demand for radar technology for civilian purposes.

The modern industrialized world is characterized by an increasing demand for automatization of industrial processes and machinery capable of operating without human supervision. Naturally, this has led to the birth of an industry of its own, focused on the design and development of high-precision sensors capable of providing fast and reliable information about their surroundings. These industrial applications place a vast range of requirements on the devices, and radars have always been promising candidates. [7]

Radars can generally be divided into pulse and continuous wave radars based on their operating principle [1]. A continuous wave radar is often frequency modulated, known as frequency modulated continuous wave (FMCW) radar. Although most of early military purpose radars were primarily pulse radars [6], continuous wave radars are not a new concept either [8].

1.2 The FMCW and pulse radar

Essentially, a radar system detects targets by transmitting a signal and then receiving echoes from its environment. Transmitted and recived signals are analyzed for collecting information about the environment. Distance to a target can be estimated from the round-trip delay acquired by processing the received signal. Round-trip delay is the time an electromagnetic wave requires to travel to a source of reflection and back to the radar. Changes to the reflected signal can be used to estimate some target parameters. These include, for example, radar cross section of the target, and its velocity. Detectable parameters have minimum and maximum values, and resolutions. These quantities depend on hardware of the radar and its type. [1]

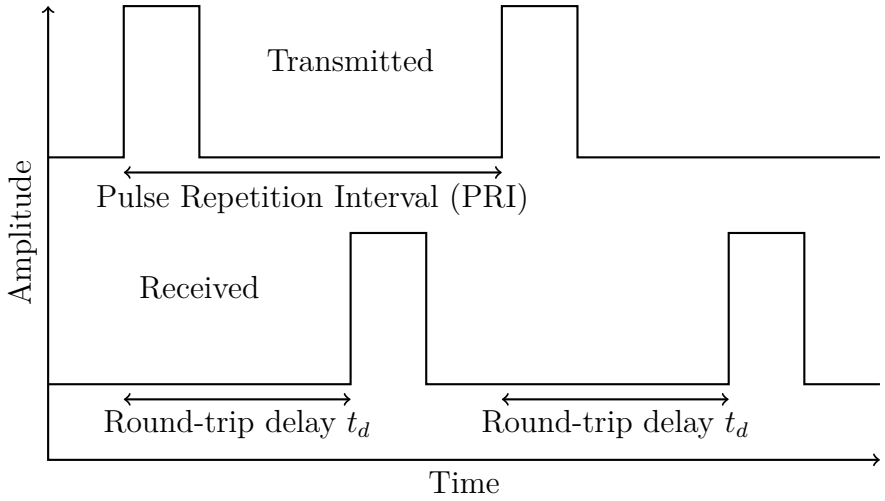

Figure 1: Simplified operating principle of a pulse radar.

A pulse radar transmits a pulse of a certain length, and detects reflections from the environment. Difference in time between the initial transmission of the pulse and the detection of a reflection can be used to determine round-trip time to the source of reflection. Power and Pulse Repetition Interval (PRI) of the radar determine how far and small a target can be while remaining detectable by the radar.

Figure 1 illustrates a simplified operating principle of a typical pulse radar. A pulse of a certain duration is transmitted, and reflected pulses from the environment are monitored. The pulse is repeated each PRI. This determines how distant a target can be while remaining detectable. Reflections must arrive before the transmission of a new pulse, otherwise they could be interpreted as close targets instead. Similarly, reflections that arrive before the transmitted pulse is finished can be difficult to detect.

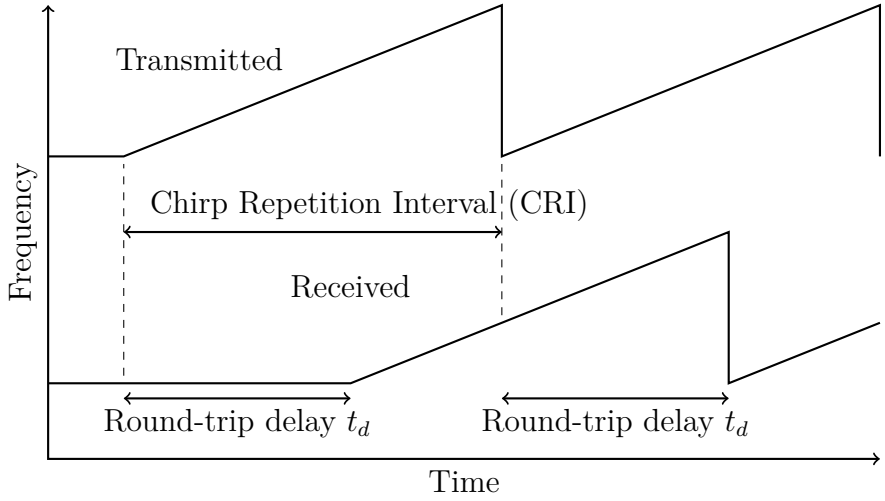

Figure 2: Simplified operating principle of an FMCW radar.

An FMCW radar differs from its pulse counterpart in that transmission and reception is continuous. Due to this, it is not possible to differentiate between transmitted and received signals in the same way as a pulse radar operates. To find the round-trip delay between transmitted and reflected signals, the signal must be modulated. This is typically achieved with frequency modulation.

An FMCW radar emits a constant carrier frequency, which is modulated to produce a waveform. The waveform may be optimized based on the situation and application [9].

Naming conventions are not uniform and can be confusing. Depending on author, the repeated waveform can be referred to as a sweep or chirp [10, 11, 6, 12], and sometimes pulse [13]. We will define sweep as the act of modulating frequency from one value to another, and a chirp as the repeated waveform consisting of one or multiple sweeps.

The sketch in Figure 2 illustratres simplified operating principle of an FMCW radar. A chirp consisting of a single linear frequency sweep is repeated each CRI. Note, that the round-trip delay is greatly exaggerated. Generally it can be expected to be only a small fraction of the chirp duration. Round trip delay can be estimated by mixing the transmitted and received signals, and assessing their frequency difference [14].

An FMCW radar has a theoretical maximum detectable distance dependent on the chirp duration. A round-trip delay longer than CRI in Figure 2 will push the received chirp to the next CRI, causing a target to appear close rather than far away. However, generally the maximum detectable distance is limited by the sampling interval of hardware. FMCW radars do not have a minimum detectable distance in the same sense pulse radars have. Rather, it is dependent on the used bandwidth. They are often preferred for short distance applications. [15]

1.3 A review of common FMCW radar applications

Radars are known to be much more robust than optical devices which are more easily affected by inclement weather and other environmental factors [16]. Due to relatively short possible operating distances and small dimensions, FMCW radars have been very popular in many civilian, industrial, and military applications. This section provides a brief overview of some popular FMCW radar applications.

1.3.1 Automotive safety

An important cause for crashes and accidents involving land-borne vehicles is a lack of situational and spatial awareness by the driver. This can range from high-velocity situations during highway merging to a slower one while reversing onto a parking spot or off a driveway. During situations like this, blind spots due to mirror placement can be dangerous. Manually monitoring blind spots requires the

driver to take their eyes off the road. Some sort of electronic monitoring system integrated into the vehicle can greatly improve driving experience. Automotive safety has long been a driving force in development of FMCW radars and their applications [17].

Automotive applications of FMCW radars are not limited to personal automotive transportation, as applications in heavy industry have been also explored. The concept and risks involving situational awareness and coordination in an environment involving multiple large vehicles and high traffic has been discussed [18]. This research has been further expanded by presenting an FMCW radar operating at 24 GHz used for close proximity detection of light vehicles [19].

Earlier modern automotive radars operated in the Industrial, Scientific and Medical (ISM) band with a center frequency of 24 GHz [20, 21], although more recent applications have been adapted to higher frequencies ranging from 76 to 81 GHz [22, 23].

1.3.2 Aviation safety

Situational awareness is extremely important on airport runways. Large and heavy vehicles must move in harmony with each other while remaining aware of their environment. Flight controllers can account for other planes leaving and entering the runway, but observing quality of the runway for small debris through visual means is difficult. The debris can be something as small as a bolt or a nut, or even a piece of concrete off the runway, and still cause extensive damage in the engines of a plane [24].

FMCW radars have been adapted in runway debris detection instead of visual recognition. Considering that a runway is supposed to be a flat and uniform surface, finding anomalies simply requires a high enough resolution. Some designs [25, 26, 27] have reached a resolution within centimeter range, and a maximum distance within hundreds of meters.

Contrary to airplanes, helicopters often fly in urban environments with tightly spaced buildings, power lines, bystanders, and with little room for error. Helicopter pilots may also find themselves in extreme weather during rescue missions, which might require landing in difficult conditions. The pilots may have their field of view severely obstructed by kicked up dust or snow in poor weather during the winter. Infrared sensors and optical devices are adversely affected by inclement weather and environmental factors. The size of dust and snow particles tends to be in the same range as wavelength of infrared [28], so millimeter wave radar is a promising technology for detection [29, 30].

1.3.3 Security

Important applications of FMCW radars are not limited to vehicles alone. Monitoring office spaces and other properties for security reasons during nights or over weekends when there is no personnel present is important. Office buildings can be locked over the night, and positioning a night guard at the reception of the building is often enough to secure an installation. However, expensive heavy equipment must often be left unattended on a construction site when work is suspended. Similarly, these sites are often used to store valuable metals, known to be frequent targets of theft.

A site can be secured with electronic equipment instead of visual surveillance. Motion detection can be realized using a continuous wave radar [31]. However, detecting people is not necessarily limited to moving persons. Luckily, humans are incapable of remaining completely still. Subtle bodily functions like breathing and heartbeat are enough to cause small changes in posture. Using an FMCW radar to detect a breathing person through obstacles has been explored earlier [32]. A similar approach could be used to detect survivors during or in the aftermath of accidents.

Applications of breathing detection are not limited to rescue missions or intruder detection alone. Reliable monitoring of breathing activity is a very important factor in the diagnosis of different problems affecting the respiratory organs. Breath activity monitoring of a patient can be performed by establishing physical contact using a device wrapped around the chest. However, they can be uncomfortable and sometimes get in the way of other operations. Medical procedures and monitoring are often sought to be as non-invasive as possible, which why wireless techniques for breath activity monitoring are desirable.

A pulse radar for monitoring breathing activity in a medical context has been proposed [33], although its range is short. The pulse radar follows movements of a patient's thorax, whereas an FMCW solution can be realized through statistical analysis [32]. Advantages of an FMCW solution are clear, as a patient moving in their bed could result in the pulse radar being misaligned.

1.3.4 Navigation assistance for the visually impaired

The cane is a very common navigation aid for the visually impaired. Specially trained seeing-eye dogs and personal caretakers are popular forms of assistance as well. However, a cane leaves its user vulnerable to obstacles that are at upper body height, or approaching rapidly. Requiring a personal caretaker or a dog may limit ones ability to travel freely.

A great variety of systems to aid a visually impaired person to navigate their surroundings have been developed [34]. Essentially, the purpose of such a device is to obtain information about the environment that normally would be acquired through vision. The information is then transformed into form that can be communicated to its wearer using some other sense.

Echolocation can be performed by means of ultrasonic or electromagnetic waves. Differences between electromagnetic radar and ultrasonic echolocators in obstacle detection for human users have been studied earlier [35]. Advantages of electromagnetic sensing compared to ultrasonic are numerous. One of them is the cosmetic factor of a navigation aid, as an ultrasonic sensors must be worn on on top of clothing. A radar device can be worn under clothing. This minimizes visibility and draws less attention to the user, reducing possible stigma of apparent visual impairment. Due to its ability to operate at short distances, FMCW radars provide a promising alternative [36, 37].

2 Linearly modulated FMCW signal

In this section, signal transmitted by the radar is discussed. Principal methods for generating frequency modulated signals are presented.

In this section, a brief mathematical description of the transmitted and received signals using a linearly frequency modulated chirp is presented. A brief discussion of relevant sources of error is also provided. After defining the linearly increasing frequency ramp, principal waveforms consisting of sweeps are presented and discussed.

2.1 Signal generation

A great range of methods exist for frequency generation. There are two principal methods of generating fast ramp FMCW chirps. One can use either a phase-locked loop (PLL) based structure, or a digital to analog converter (DAC) based structure [38]. A hybrid of the two methods has also been considered [39].

The DAC implementation is based on a direct digital synthesizer (DDS), which consists of a phase accumulator, a look up table (LUT), and the DAC. The phase accumulator is connected to a LUT which converts phase to a digital amplitude. The DAC converts this to an analog current. For more details on operation of a DDS, see [40].

The second implementation based on a PLL consists of a closed loop structure. For details on its operation, see [41]. Due to the nature of the closed loop, non-linearity compensation is not required when using a PLL architecture. This is also the architecture of choice for the radar device used during this work. Due to its high linearity [42, 43, 44], it can be assumed that error due to non-linearity is negligible.

When generating a short chirp, DAC is more advantageous as it does not require a settling time. PLL will experience over- and undershoot [28]. This effect will

become more pronounced the shorter a chirp is, or the more rapidly it must change, e.g. for a sawtooth wave. However, it has been concluded that the chirp durations used in this work are sufficiently long in duration and therefore do not suffer from this significantly. By careful choice of the waveform, the possibility of over- and undershoot can be reduced further. Namely, by favouring triangular waveform over either a linear ramp or a sawtooth. A triangular waveform has no steep drop back to the carrier frequency, which will be demonstrated in the following section.

2.2 Mathematical description

Mathematical description of a linearly modulated FMCW signal is presented here, along with the relevant frequency components due to a single target [45].

Consider a linearly increasing frequency ramp that is swept from a carrier frequency f_c across a bandwidth of B to value of $f_c + B$. The frequency at time t for each sweep can be expressed as

$$f(t) = f_c + \frac{Bt}{T}, \tag{1}$$

where T is duration of the sweep. Phase corresponding to the signal frequency is the integral of Equation (1) with respect to time, or

$$\phi(t) = 2\pi(f_c t + \frac{Bt^2}{2T}). \tag{2}$$

Transmitted sinusoidal signal with a linearly changing frequency can now be expressed as

$$u_{\mathrm{Tx}}(t) = \cos\left(2\pi f_c t + \frac{\pi B(t - mT)^2}{T}\right). \tag{3}$$

It assumed that sweeps are performed continuously. First term inside the cosine function corresponds to phase shift due to the carrier frequency, and second term due to the modulated frequency. Term $t - mT$ must be substituted to calculate frequency for m^{th} sweep. A normalized amplitude of 1 is assumed from this point onward.

Let us now assume a target at distance R, moving at a radial velocity of V at time t. Radial velocity is defined as being positive when a target is moving away from the radar, and as negative when it is moving towards the radar. A chirp reflected from the target is assumed otherwise the same as the transmitted signal, but delayed by a round-trip delay of

$$t_d = \frac{2(R + Vt)}{c}, \tag{4}$$

where c is speed of light in the medium of propagation. The returned signal also has its amplitude decreased due to the distance R. Since only frequency components are of interest, the term will be omitted for the sake of clarity.

Returned signal for m^{th} sweep is therefore given by

$$u_{\mathrm{Rx}}(t) = \cos\left(2\pi f_c(t - t_d) + \frac{\pi B(t - t_d - mT)^2}{T}\right). \tag{5}$$

Received signal is mixed with the transmitted signal. Based on familiar trigonometric identity

$$\cos(a)\cos(b) = \frac{1}{2}(\cos(a+b) + \cos(a-b)), \tag{6}$$

it can be deduced that mixing and subsequent summation of the frequencies will result in a very high frequency component on the order of $2f_c$. It is essential to use a low-pass filter to get rid of this component, leaving only the much lower difference frequency. Mixed and filtered signal can therefore be expressed as

$$u_m(t) = u_{\mathrm{Tx}}(t)u_{\mathrm{Rx}}(t) = \frac{1}{2}\cos\left(2\pi f_c t_d + \frac{2\pi B}{T}t_d(t - mT) - \frac{\pi B t_d^2}{T}\right). \tag{7}$$

Substituting Equation (4) to Equation (7) results in

$$u_m(t) = \frac{1}{2}\cos\left(\frac{4\pi f_c(R+Vt)}{c} + \frac{4\pi B(R+Vt)(t-mT)}{cT} - \frac{4\pi B(R+Vt)^2}{c^2 T}\right). \tag{8}$$

This mixed and filtered signal can be processed to estimate range and radial velocity of the source of reflection.

First, third term of the cosine in Equation (8) can be assumed to be sufficiently small due to c^2 to ignore completely. Second, by expanding the remaining two terms we get

$$u_m(t) = \frac{1}{2}\cos\left(2\pi\left(\frac{2f_cR}{c} + \frac{2f_cV}{c}t + \frac{2BR}{cT}t - \frac{2BRmT}{cT} + \frac{2BV}{cT}t^2 - \frac{2BVmT}{cT}t\right)\right). \tag{9}$$

Let us now define t' to be time from the start of sweep number m,

$$t = mT + t'. \tag{10}$$

This is done to simplify signal processing later. This definition is substituted into Equation (9). By expanding the second power, we get

$$\begin{aligned} u_m(t') = \frac{1}{2}\cos\Bigg(2\pi\Bigg(&\frac{2f_cR}{c} + \frac{2f_cV}{c}(mT+t') + \frac{2BR}{cT}(mT+t') - \frac{2BRmT}{cT} \\ &+ \frac{2BV}{cT}(m^2T^2 + 2mTt' + t'^2) - \frac{2BVmT}{cT}(mT+t')\Bigg)\Bigg) \end{aligned} \tag{11}$$

Assuming the sweeps are sufficiently short, the terms dependent on second power of t' can be assumed to be negligible. The expression can now be rearranged into

$$u_m(t') = \frac{1}{2}\cos\left(2\pi\left(\frac{2f_cR}{c} + \frac{2f_cVmT}{c} + \left(\frac{2f_cV}{c} + \frac{2BR}{cT} + \frac{2BVm}{c}\right)t'\right)\right) \tag{12}$$

It is now assumed that the radial velocity of the target is sufficiently slow so that range R remains constant for each sweep. First term inside the cosine is assumed a constant phase term for all sweep numbers, and ignored. The signal now contains

a progressive phase shift as a function of m, and a frequency component. We will momentarily refer to the frequency as peak frequency of the signal. The signal can be expressed more compactly as

$$u_m(t') = \frac{1}{2}\cos\left(2\pi\left(f_p t' + f_d m T\right)\right), \tag{13}$$

where two new terms have been defined as

$$f_d = \frac{2 f_c V}{c}, \tag{14}$$

$$f_p = \frac{2BR}{cT} + f_d + \frac{2BVm}{c} = f_b + f_d + f_m. \tag{15}$$

Quantities f_d and f_b are known as the Doppler and beat frequencies of a specific target.

It can be seen that the peak frequency f_p is determined by the range R of the target, its radial velocity V and the sweep number m. First term is simply frequency difference between transmitted and returned chirps due to round trip delay. Second term is due to the reflected signal becoming either compressed or elongated based on whether the target is moving away or towards the detector. Third term accounts for the target moving over the course of a number of sweeps, if multiple sweeps are analysed.

Effect of sweep number can generally be assumed to be negligible. For purposes of signal processing, it is also customary to assume that effect of f_d on the peak frequency is small enough to ignore. Range information can therefore be estimated from the resulting frequency component. Relation between beat frequency and range is

$$f_b = \frac{2BR}{cT}, \tag{16}$$

or rearranged to solve for R

$$R = \frac{cT f_b}{2B}. \tag{17}$$

For increased accuracy, range estimation can be adjusted by taking f_d and f_m into account, after the radial velocity has been estimated.

2.3 Error sources

2.3.1 Frequency shift due to radial velocity and sweep number

R [m]	1	2	3	4	5
f_b [Hz]	6,670	13,300	20,000	26,700	33,400
V [m/s]	1	2	3	4	5
f_d [Hz]	160	320	480	640	801
f_m [Hz], $M = 32$	53.4	107	160	213	267

Table 1: Frequency values of beat frequency components calculated for a range of target distances and velocities. Values calculated for a typical device with $f_c = 24$ GHz, $B = 250$ MHz, $T = 250$ µs. Total number of sweeps $M = 32$.

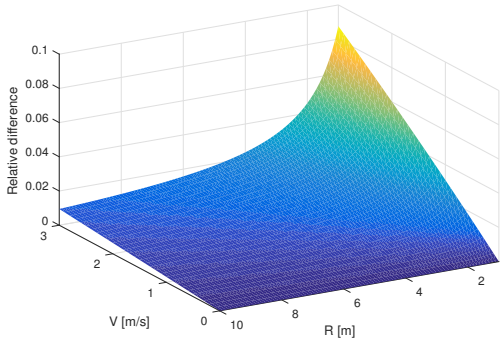

Figure 3: Relative difference in frequency as a function of R and V between f_b and $f_b + f_d + f_m$. This translates to an error of same magnitude in estimated distance to the target. Values calculated for a typical device with $f_c = 24$ GHz, $B = 250$ MHz, $T = 250$ µs. Total number of sweeps $M = 32$.

The Doppler shift of frequency is linearly dependent on radial velocity of the source of reflection. This applies to f_m as well, which is in addition dependent on the sweep number. It is clear that the faster a target moves, the higher the error resulting from ignoring f_d and f_m is going to be. Table 1 provides a snapshot of frequency component values calculated for a typical FMCW radar operating for short ranges. Since the resulting frequencies are dependent on parameters of both the target and radar device, they were calculated for a typical device.

As can be seen, beat frequency can easily be assumed to almost always be in the kilohertz range, whereas the Doppler component is only in the hundreds of hertz range. Similarly, the sweep component can also be seen to be relatively small even after 32 sweeps.

This is further illustrated in Figure 3, which shows the effect of ignoring Doppler and sweep terms of the peak frequency. Assuming the terms have no effect on the

peak frequency results in the entire peak frequency being converted to range. This results in an error in estimated distance to the target.

It can be seen that a longer distance to a target will result in lower relative error. Conversely, increased target radial velocity will consequently increase the error. A target moving at a typical walking speed of between 1 and 3 meters per second may result in up to 10% error in estimated range. The highest error will be produced by a fast moving target close to the radar. Depending on the required precision, this may be an acceptable margin of error.

It should also be noted that once the radial velocity of a target has been determined, this information may be used to correct the previous estimations of target position. The same applies to sweep number term f_m. However, this introduces additional computational steps.

Note that these values were calculated for a case when a total of $M = 32$ sweeps had been collected. For a lower number of sweeps, the effect of f_m will be lower. If only one sweep is performed and analyzed, it has no effect at all, and the error will be only due to the Doppler shift.

2.3.2 Non-linearity of the sweep

The reliability of estimated target parameters depends also on the linearity of the frequency modulation. A highly linear frequency sweep is a requirement of accurate measurements [46]. Non-linearities of the sweep will introduce a systematic bias in estimated target parameters [47], as well as degraded measurement resolution, variance in estimations, and widening of the frequency peak corresponding to a target [48].

A number of methods have been developed for correcting effects of sweep non-linearity [10, 49, 50]. These methods and their implementations are complicated, and may require either additional steps in signal processing or new components.

2.4 Waveforms

2.4.1 Ramp

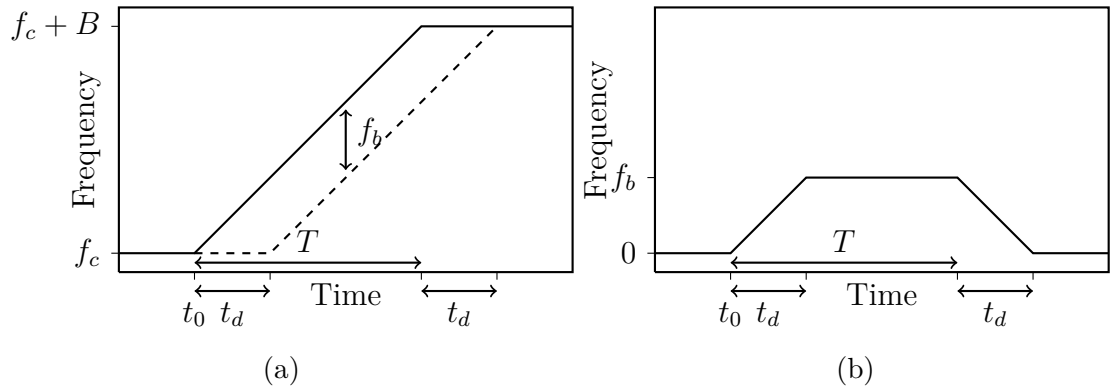

Figure 4: (a) Frequency of transmitted and received ramp chirps as a function of time, and (b) the resulting beat frequency as a function of time.

Consider a ramp function triggered at moment $t = t_0$, which rises from value f_c to $f_c + B$ over a time interval of T. The carrier frequency of the chirp is denoted by f_c, bandwidth of the sweep by B, and chirp duration by T.

A simple sketch of a ramp modulation scheme is illustrated in Figure 4a. The solid line represents the frequency of the transmitted signal as a function of time, and the dashed line the same for a reflected signal from a single stationary target. The delay caused by the transmitted pulse having to travel to the target and back is denoted by round-trip delay t_d.

Figure 4b illustrates the resulting beat frequency as a function of time. It can be seen that a fall and rise time equal to the round-trip delay t_d is required for the beat frequency to reach a value that can be used to estimate distance to the target.

It should be noted that the illustrations here have greatly exaggerated x-axes for the sake of clarity. In reality, the round-trip delay will be in the order of tens of nanoseconds for targets at distances of up to about 100 meters. Assuming the chirp duration on the order of hundreds of microseconds, the delay will be insignificantly short. Still, for this method to work at all, the delay absolutely has to be shorter than duration of the chirp.

Clearly, frequencies resulting from the rise and fall times are useless. It is therefore wise to formulate sampling of the signal so that most of the samples can be trusted to fall on the section with a constant beat frequency.

2.4.2 Sawtooth

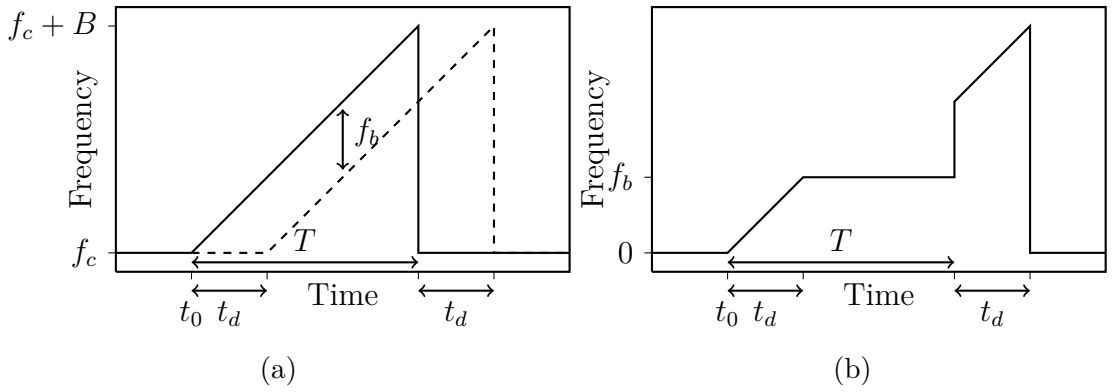

Figure 5: (a) Frequency of transmitted and received sawtooth chirps as a function of time, and (b) the resulting beat frequency as a function of time.

A sawtooth is very similar to a ramp function. Their difference is that after the bandwidth has been swept, the frequency is immediately returned to the carrier frequency.

A sketch of the waveform is illustrated in Figure 5a. Notation here is the same as for the ramp function. The sawtooth waveform requires a rapid change in frequency after the ramp has been completed. A rapid change in frequency can result in an undershoot [38].

Over- and undershoot becomes more of a problem for shorter times between each chirp. This can also cause difficulties if the application is tightly limited to a certain bandwidth.

Figure 5b illustrates resulting beat frequency as a function of time. Its behaviour is very similar to ramp function, except there is a segment with a much higher frequency. It can be avoided by leaving short time margins near start and end points of the chirp.

2.4.3 Triangular

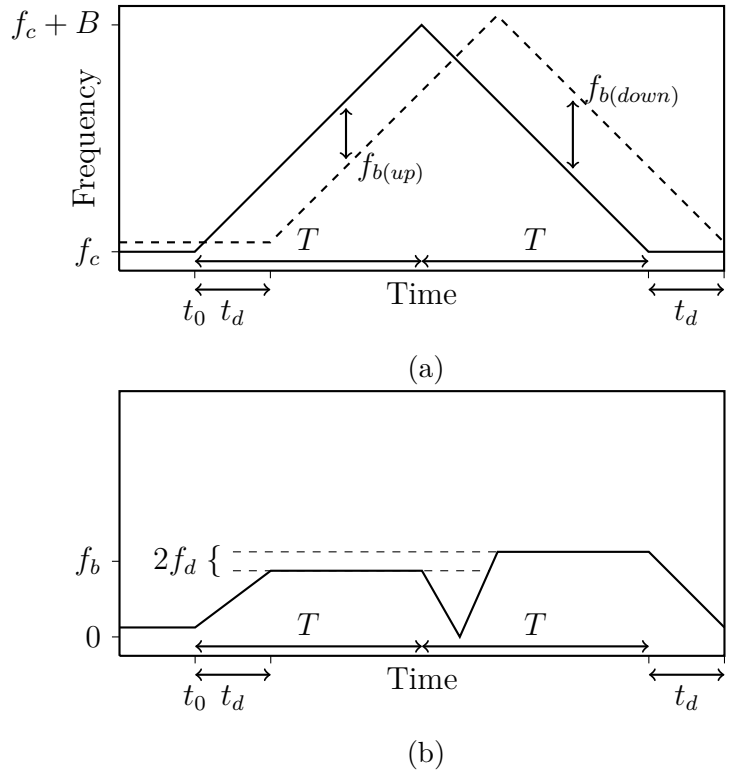

Figure 6: (a) Frequency of transmitted and received triangular chirps as a function of time, and (b) the resulting beat frequency as a function of time.

Looking back on chirps consisting of either a single ramp or sawtooth function, a clear weakness can be identified. Each received chirp essentially contains two unknown quantities, range and radial velocity of a target. It is not feasible to estimate both of them from a single chirp, which is why the Doppler shift is often initially ignored. By introducing an additional linear ramp section of opposite slope to the chirp to form a triangle [51], it is possible to estimate both quantities from a single chirp.

Figure 6a illustrates a transmitted and received triangular chirp. The chirp consists of two ramps of opposite slope, both with a duration T. The received chirp is delayed by a round-trip delay required for the signal to travel to a target and then back. Note that the received chirp is now drawn with a small positive Doppler shift. This is due to the shift being fairly straightforward to calculate, contrary to the previous two waveforms.

Two assumptions must be made, which are reasonable depending on the application. Firstly, radial velocity of the target must remain relatively constant over full duration of the chirp. Secondly, it must also be sufficiently low so that the target does not move significantly over full duration of the chirp.

The entire chirp experiences a Doppler shift. If the shift is positive, the beat

frequency is decreased for the rising section of the chirp, and increased for the falling section. The opposite stands for a negative Doppler shift. This can be seen illustrated in Figure 6b. Up and down ramp sections are affected by the Doppler shift with opposite signs.

For this particular example, the two beat frequencies are

$$f_{b,\text{up}} = f_b - f_d = \frac{2BR}{cT} - \frac{2Vf_c}{c}, \tag{18}$$

$$f_{b,\text{down}} = f_b + f_d = \frac{2BR}{cT} + \frac{2Vf_c}{c}. \tag{19}$$

The Doppler shift can be calculated fairly straightforwardly from difference between the two peaks,

$$f_d = \frac{f_{b,\text{down}} - f_{b,\text{up}}}{2}. \tag{20}$$

Similarly, the unshifted beat frequency can be calculated from mean of the up and down ramp section beat frequencies. Summation cancels Doppler components out, and the unshifted beat frequency can hence be expressed as

$$f_b = \frac{f_{b,\text{down}} + f_{b,\text{up}}}{2}. \tag{21}$$

Using two opposite linear ramps it is therefore possible to estimate both the range and the radial velocity of a target with one chirp. Correcting the range of the target is not necessary, as Doppler shift is already cancelled out from the estimation.

3 FMCW radar signal processing

Estimating target parameters with an FMCW radar is based on analysis of signal resulting from a mix of the transmitted and received chirps. Multiple methods exist for accurately analyzing data acquired with an FMCW radar. These include, for example, the chirp z-transform [52, 53], and the ESPRIT algorithm [54].

The following implementations are based on the Fast Fourier Transform (FFT). Estimating target parameters based on frequency components in the signal is simply a matter of finding local maximums from absolute value of the signal spectrum. It is also possible to estimate target parameters based on phase of the signal [55, **?**, 56, 57]. This can be done either separately or in addition to frequency for an improved accuracy.

This section discusses processing the received signal. As was pointed out earlier, estimating both range and radial velocity of a target from a single linear ramp chirp is not feasible. Rather, the slightly more complex method of slow-time processing [14] is required. Multiple sweeps are performed, and radial velocity of a target is estimated based on a gradual phase shift due to its movement.

Method of slow-time processing is outlined over the next few pages. Signal processing a triangular chirp will also be discussed and contrasted. Resolution, accuracy, and computational complexity are points of contention between these methods.

3.1 Slow-time processing

A number of chirps are collected and stored in a raw-data matrix. Assuming M chirps are performed, and each of them is represented by N samples, this results in a $M \times N$ matrix.

The matrix is processed by performing two sets of FFTs. The first set is performed along rows of the matrix, or for each chirp individually. This extracts frequency information from the chirps, which can be converted into range information. The second set is performed along columns of the matrix. This will be shown to extract information about phase of each frequency component, which can be converted into information about radial velocity of each corresponding target.

3.1.1 Extracting range information with a single ramp chirp

The first set of FFTs are perfomed individually to each performed chirp.

After the transmitted and received signals have been mixed, the corresponding frequency spectrum can be obtained by performing an FFT. The mixed signal given in Equation (13) is sampled in N points over the chirp period T, so that

$$NT_s = T, \tag{22}$$

where T_s is the sampling period. The signal is therefore sampled at times

$$0,\ T_s,\ 2T_s\ , \ldots, (N-1)T_s. \tag{23}$$

After the FFT, the spectrum will consist of frequencies

$$-\frac{N}{2T},\ (-\frac{N}{2}+1)\frac{1}{T}, \ldots, 0, \ldots, (\frac{N}{2}-1)\frac{1}{T}. \tag{24}$$

For the sake of simplicity, finite and discrete nature of the sampled signal is momentarily ignored. Let us now reconsider the mixed signal derived earlier,

$$u_m(t') = \frac{1}{2}\cos\Big(2\pi\Big(f_b t' + f_d m T\Big)\Big). \tag{25}$$

It can be seen that the signal contains a frequency component of f_b and a phase shift of $f_d m T$. Using the familiar Fourier identity of a delayed cosine function, FFT of the signal can be expressed as

$$\mathrm{FFT}(u_m(t'))[f] = U_m = \frac{1}{4}\exp(2\pi i f_d m T)\delta(f-f_b) + \frac{1}{4}\exp(-2\pi i f_d m T)\delta(f+f_b). \tag{26}$$

The spectrum can be seen to contain two peak frequencies with equal magnitude and opposite sign. They also have a phase shift of equal magnitude and opposite sign. The phase shift is linearly dependent on chirp number m. The phase shift is crucial in extracting Doppler information from the sampled signals.

3.1.2 Resolution and maximum value of range estimation with a single ramp chirp

Converting the spectrum into range information is as simple as using

$$R = \frac{cTf_b}{2B} \tag{27}$$

to calculate distance corresponding to each frequency point. This will result in a set of range cells given by

$$\frac{cN}{4B}, \frac{c}{2B}(\frac{N}{2} - 1), \ldots, 0, \ldots, \frac{c}{2B}(\frac{N}{2} - 1). \tag{28}$$

It is clear that due to discrete nature of the time series, range information will also be represented in steps. Range resolution of the measurement is given by

$$\Delta R = \frac{c}{2B}. \tag{29}$$

An interesting observation is that the range resolution is dependent only on the swept bandwidth. Targets within the same range cell will be indistinguishable from each other Similarly, the maximum range can be calculated from

$$R_{\max} = \frac{cN}{4B}. \tag{30}$$

Note that this maximum value is dependent on the number of samples and sampling interval, and is determined by hardware. As was pointed out in Section 1.2, the actual maximum limit relates to chirp duration, and can be expressed as

$$R_{\max} = \frac{cT}{2}. \tag{31}$$

This is the distance that corresponds to a round-trip delay equal to chirp duration T, and can be in the order of several kilometers, while the hardware dependent maximum distance is in the order of tens of meters. It can generally be assumed that the limiting factor in maximum detectable range is hardware instead of chirp duration and round-trip delay. From now on it is assumed that Equation (30) is in effect.

The maximum range allows us to find the largest beat frequency that can be detected. Substituting maximum distance Equation (27), we get

$$f_{b,\max} = \frac{2BR_{\max}}{cT} = \frac{N}{2T}. \tag{32}$$

Based on the Nyquist sampling theorem, required sampling period as a function of the desired maximum detectable distance is

$$T_s = \frac{1}{2f_{b,\max}} = \frac{cT}{4BR_{\max}}. \tag{33}$$

Targets further than the maximum distance defined here will result in a beat frequency that is higher than the maximum detectable frequency. This will result in aliasing of the signal spectrum.

This section presented the signal processing method for extracting range information from a sampled chirp. The measurement is limited by the highest detectable distance and the range resolution of the measurement.

It is possible to accurately estimate position of a target if it is moving sufficiently slow. This way beat frequency is not distorted by Doppler shift. The radial velocity of a target can be estimated with only one chirp and FFT by comparing its positions over time. However, this would be a very cumbersome process and would require specific targets to be tracked over multiple chirps. It is often necessary to acquire instantaneous information about position and velocity of a target.

For more accurate and instantaneous radial velocity estimation, the Doppler shift of the returned chirp must be analysed. A second round of FFTs and multiple sweeps are needed for slow-time processing.

3.1.3 Extracting radial velocity information with slow-time processing

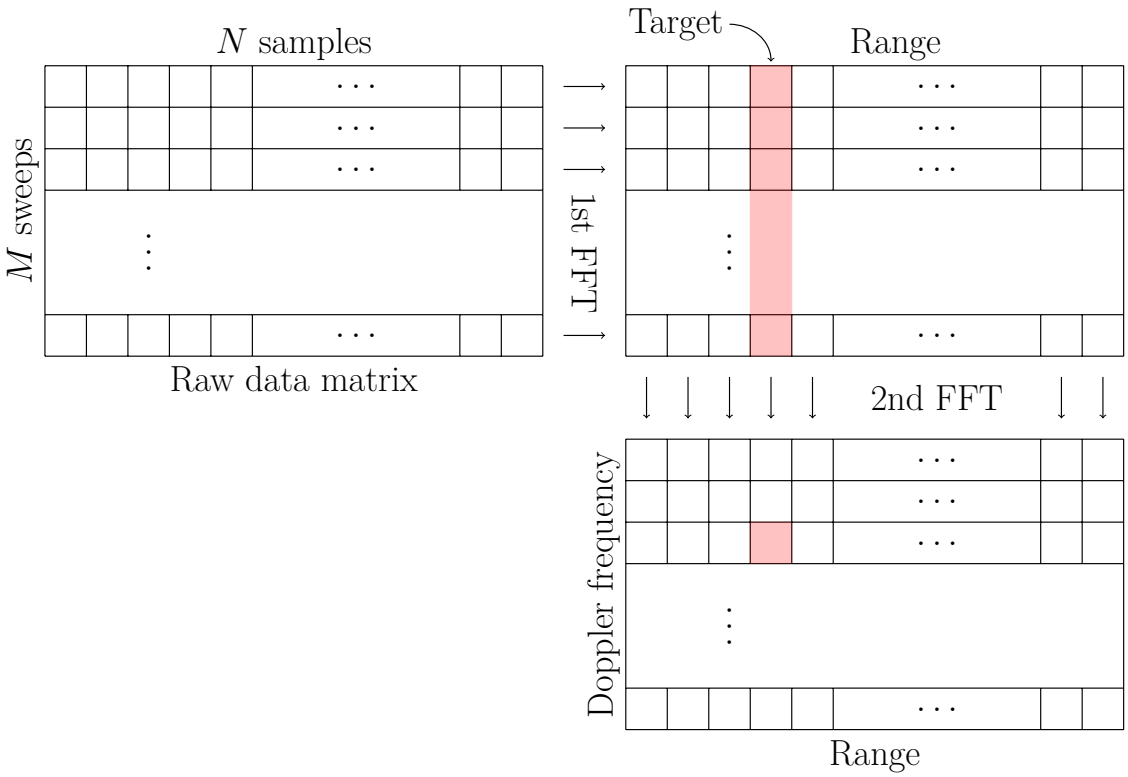

Figure 7: Illustration of the slow-time processing required to find Doppler frequency of a target.

To find the Doppler component corresponding to a moving target, a second round of FFTs is required. A number of chirps are transmitted, and resulting mixing signals sampled before signal processing. Number of sweeps M is often some power of two. The sampled chirps are stored in a $M \times N$ raw data matrix, with M rows for each chirp, and N columns for each sample in time.

An FFT is performed on each individual chirp. This step is illustrated in Figure 7 as the 1st FFT. A target should appear as a peak frequency in each row. Due to the target movement while M chirps are being collected, the successive peak frequencies exhibit a gradual phase shift. The phase shift is linearly dependent on the sweep number and Doppler frequency. Phase shift was identified as an exponential function in Equation (26).

It is assumed that the radial velocity of the target is sufficiently low as not to cause it to shift from one range bin to another over the course of M chirps. A second round of FFTs is performed, this time along columns of the data matrix. This should yield the Doppler frequency of a target in a specific range bin.

$$\begin{array}{cccccccc} & -f_{b,\max} & \cdots & f=-f_b & \cdots & f=f_b & \cdots & f=f_{b,\max} \\ m=0 & 0 & & \frac{1}{4} & & \frac{1}{4} & & 0 \\ n=1 & 0 & \cdots & \frac{1}{4}\exp(-2\pi i f_d T) & \cdots & \frac{1}{4}\exp(2\pi i f_d T) & \cdots & 0 \\ m=2 & 0 & & \frac{1}{4}\exp(-2\pi i f_d 2T) & & \frac{1}{4}\exp(2\pi i f_d 2T) & & 0 \\ \vdots & & & \vdots & & \vdots & & \vdots \\ m=M & 0 & \cdots & \frac{1}{4}\exp(-2\pi i f_d MT) & \cdots & \frac{1}{4}\exp(2\pi i f_d MT) & \cdots & 0 \end{array} \tag{34}$$

The data matrix after the first set of FFTs is presented in Equation (34). The matrix illustrates a situation where one moving target has been detected at beat frequency f_b.

Row $m = 0$ shows FFT of the first chirp. Two peak frequencies at the opposite signs can be seen. Over the course of collecting M chirps, each represented by its own row, the target remains in the same frequency bin. The peak frequency exhibits a changing phase linearly dependent on the sweep number m, the Doppler frequency resulting from the movement, and the chirp duration T.

Next, an FFT is performed along the columns of the data matrix. The columns can be treated simply a time series with a sampling period of T.

$$\begin{array}{cccccccc} & -f_{b,\max} & \cdots & f=-f_b & \cdots & f=f_b & \cdots & f=f_{b,\max} \\ -\frac{1}{2T} & 0 & & 0 & & 0 & & 0 \\ \vdots & & & \vdots & & \vdots & & \vdots \\ -f_d & 0 & \cdots & \frac{1}{4} & \cdots & 0 & \cdots & 0 \\ \vdots & & & \vdots & & \vdots & & \vdots \\ f_d & 0 & \cdots & 0 & \cdots & \frac{1}{4} & \cdots & 0 \\ \vdots & & & \vdots & & \vdots & & \vdots \\ \frac{1}{2T} & 0 & \cdots & 0 & \cdots & 0 & \cdots & 0 \end{array} \tag{35}$$

Data matrix after the second set of FFTs is presented in Equation (35). Based on the well-known Fourier transform of an exponential function, it is clear that an FFT along the columns $\pm f_b$ will produce single peaks corresponding to $\pm f_d$ with equal magnitudes.

Both range and radial velocity of a target can thus be estimated with what is essentially a two-dimensional FFT. Certain assumptions have been made in this process. Firstly, the discrete nature of the sampled signals was temporarily ignored for the sake of clarity. The real spectrum of a sampled signal is obviously not going to produce a single frequency peak as was assumed here, but rather a more spread one.

Secondly, while deriving an expression for the mixed signal, it was assumed that the constant phase terms and quadratic time dependence had a negligible effect. This allowed the signal to be reduced only to a beat frequency and Doppler frequency dependent phase shift.

Thirdly, assumptions were made about the radial velocity of the target. The radial velocity was assumed constant across the MT long period of gathering all required. The radial velocity of the target was also assumed to be low enough as not to move from one range bin to another.

3.1.4 Resolution and maximum value of estimated radial velocity with slow-time processing

The second round of FFTs is performed on a time series with a sampling interval of T. This means that a detectable Doppler frequency is limited by the Nyquist criterion. Maximum Doppler shift due to the criterion can be expressed as

$$f_{d,\max} = \frac{1}{2T}. \tag{36}$$

The maximum radial velocity can be found by inserting maximum Doppler shift into Equation (14) and solving for V, resulting in

$$V_{\max} = \frac{c}{4f_cT}. \tag{37}$$

Along with the maximum detectable radial velocity, an important factor is the resolution of the radial velocity. From Equation (35) it can be seen that the resolution is determined by the length of the second FFT along columns of the data matrix. The frequency resolution along the columns can be calculated from highest the detectable Doppler frequency and the length of the FFT. Frequency resolution is inserted into Equation (14), and when solving for V radial velocity resolution is given by

$$\Delta V = \frac{c}{2f_cMT}. \tag{38}$$

Table 2: Measurement parameters of a device with $f_c = 24$ GHz, $B = 250$ MHz, $T = 250$ µs, and total sweep number $M = 32$.

$V_{\max}$	ΔV	$R_{\max}$	ΔR
12.5 m/s	0.781 m/s	25.6 m	0.60 m

Consider a device with the same parameters as in previous examples. A sampling period of $T_s = 2.925$ µs is assumed, resulting in $N = 90$ samples to cover a single chirp. Resulting measurement parameters are presented in Table 2. A total of $M = 32$ chirps are collected for slow-time processing, resulting in a total duration of 8 milliseconds. Note that intermediary time required for storing the data and other relevant processes are not included in these calculations. Due to this, CRI is often used over T. Since CRI is dependent on hardware, T is used in these calculations instead.

These parameters will clearly result in a very good resolution when approximating

the radial velocity of a target. However, maximum radial velocity might prove problematic in some applications. Especially for highway speeds, the maximum detectable radial velocity of approximately 45 km/h is very low. Same applies to the maximum detectable range.

The maximum detectable radial velocity can be increased with either a lower carrier frequency or shorter chirp duration. The carrier frequency and bandwidth of the device are dependent on hardware, so changing them might prove difficult. They are also subject to regulation. A shorter chirp will result in proportionally worse resolution. Conversely, the resolution can be increased by gathering a higher number of chirps. This will increase the total time required to gather the raw data matrix and process it.

3.2 Processing a triangular chirp

Due to linear relation between frequency components of the mixed signal and target parameters, FMCW modulation schemes are often based on linearly increasing ramps. Combining chirps with multiple slopes has been shown to be an effective method for estimating both range and radial velocity of multiple targets [58, 59, 9].

Refer back to a sketch of the triangular chirp presented in Figure 6. Up and down sections of the triangular chirp will produce slightly different beat frequencies for a moving target, as the Doppler shift affects them with opposite signs.

When using a triangular chirp, the resolution and maximum values of detectable range are the same as outlined in Section 3.1.2. This is because a triangular chirp is just two consecutive ramps with an opposite slope.

3.2.1 Resolution and maximum value of estimated radial velocity with a triangular chirp

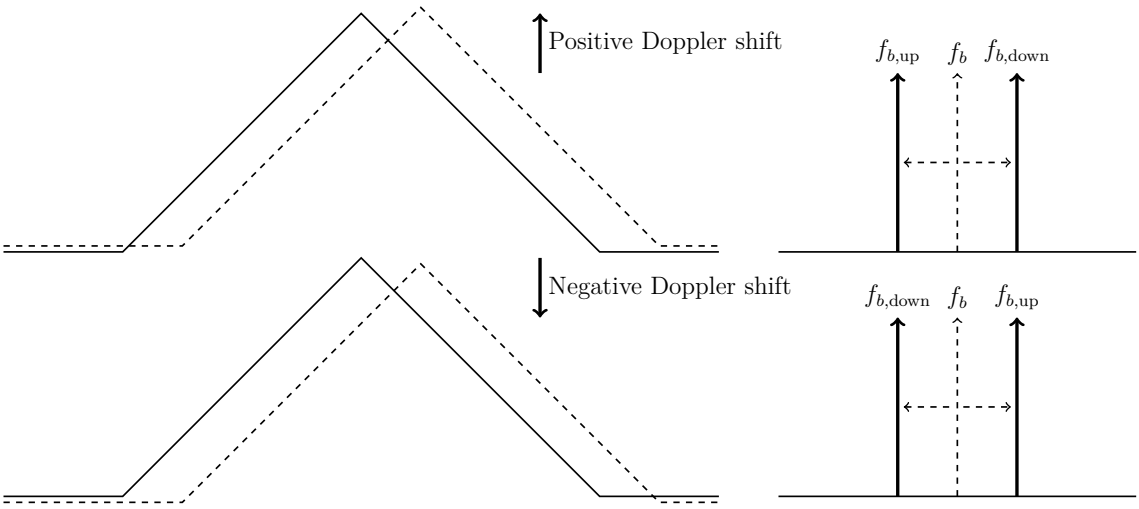

Figure 8: Effect of Doppler shift on frequency peaks when target is either moving towards or away from the radar. Solid line represents transmitted and dashed received chirp. On the right a sketch of the spectrum, with up and down

Consider a triangular chirp reflected from a moving target. As stated earlier, a Doppler shift will cause beat frequencies from up and down ramps of the triangular chirp to drift apart. Their directions depend on whether the target is moving away from or towards the target. The unshifted beat frequency lies between them. This is illustrated in Figure 8.

Because the Doppler frequency is calculated from the same spectrum as the beat frequency, its maximum value is not as limited as with slow-time processing. Up and down ramp section beat frequencies are free to shift apart until they become aliased.

The highest margin for Doppler shift is when the target is halfway over $R_{\max}$. This is where up and down section beat frequencies have the most space to shift apart.

The beat frequency corresponding to $R_{\max}/2$ is

$$\frac{f_{b,\max}}{2} = \frac{BR_{\max}}{cT}. \tag{39}$$

This can be used to calculate a radial velocity that causes the corresponding Doppler shift,

$$V_{\max} = \frac{BR_{\max}}{2f_cT}. \tag{40}$$

Furthermore, we may insert $R_{\max}$ in terms of the sampling interval T_s to reduce the maximum radial velocity to

$$V_{\max} = \frac{c}{8 f_c T_s}. \tag{41}$$

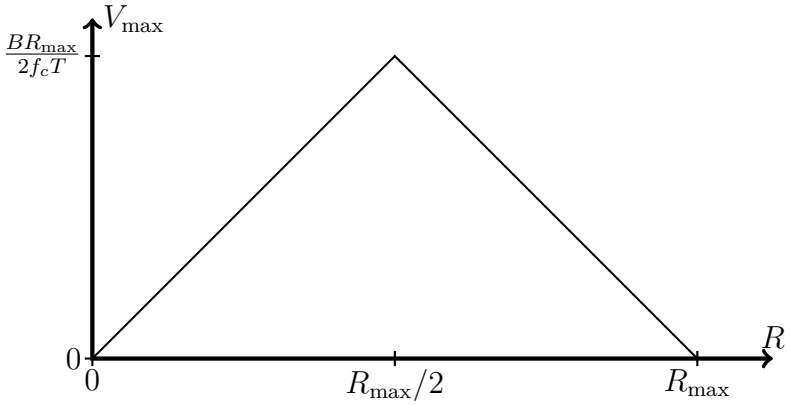

Figure 9: Maximum detectable radial velocity as a function of target distance in relation to $R_{\max}$.

A theoretical maximum can be calculated for the radial velocity. Margin by which up and down beat frequencies can drift apart before becoming aliased depends on target position.

The described effect on maximum detectable target radial velocity is illustrated in Figure 9. The maximum detectable radial velocity will decrease linearly towards zero as the target moves away from the halfway point, and there is less space for the up and down section frequencies to drift apart before they become aliased.

This suggests that the radial velocity estimated with a triangular chirp is much less limited in terms of its maximum value, than when done with slow-time processing. It is reasonable to assume that most applications using a triangular chirp will rarely be limited by $V_{\max}$.

The radial velocity resolution of measurements with a triangular chirp is another factor by which it differs from slow-time processing. Previous works [51, 60, 61] have suggested that the radial velocity resolution is given by

$$\Delta V = \frac{c}{2 f_c T}, \tag{42}$$

where T is duration of one ramp section, and therefore half of full duration of the triangular chirp. This expression results in a Doppler frequency resolution of

$$\Delta f_d = \frac{1}{T}, \tag{43}$$

which implies that the smallest detectable change in Doppler frequency is inversely proportional to the duration of the chirp. For a Doppler frequency to be detectable,

entire period corresponding to the frequency would have to be sampled.

This appears to be quite an unforgiving limitation. For example, triangular chirps using single ramps shorter than 500 microsecond would be capable of detecting Doppler frequencies of only 2 kHz and higher. This in turn would translate to a radial velocity resolution of 12.5 m/s, which would be an impractically coarse resolution for many applications.

3.3 A comparison of triangular chirp and slow-time processed single ramp chirps

3.3.1 Required computations

Consider first slow-time processing of multiple ramp chirps. After a number of chirps have been transmitted, two sets of FFTs are performed. This is essentially a two-dimensional FFT. First round is to find the range information of potential targets. The second is to find the phase shift and Doppler frequency due to target movement.

Contrary to slow-time processing single ramp chirps, only one triangular chirp is processed for each target parameters estimation. This means that at the very least one FFT is performed, but generally two. Up and down ramp sections of a triangular chirp are often analyzed separately [9, 62, 63]. This will be the case in the presented implementation as well.

Separate analysis presents an additional problem in the form of correctly pairing frequencies corresponding to a real target. In a multiple target situation, N targets result in N frequency peaks in both up and down ramp section FFTs. While a large number of combinations exist for them, naturally only N of them correspond to real targets. False pairings result in ghost targets [60, 64, 65], which do not correspond to a physical source of reflection. Depending on application, these may be especially dangerous.

To solve this problem, much time has been dedicated to the study of frequency pairing algorithms [66, 62, 67, 68]. To simplify the pairing process and reduce number of potential ghost targets, modifications have been proposed to the triangular waveform. Namely, some of these include trapezoidal waveform [63], waveforms with alternating slopes [69, 66], combinations of multiple waveforms [64], and combinations of stepped and linear frequency modulation [70].

These efforts can be contrasted with the fact that for a 2D FFT, pairing of beat frequencies to a specific Doppler shift is essentially implicit [71, 68, 72]. Pairing algorithms and elimination of ghost targets will not be considered further in this

thesis, as all measurements were focused on estimating parameters of a single target.

It should also be kept in mind that beat frequencies acquired with slow-time processing are Doppler shifted, if their corresponding targets are moving. This may require an additional step in computations to correct. Each beat frequency needs to be adjusted with the corresponding Doppler frequency. Contrary to this, calculating the beat frequency from up and down sections of a triangular chirp eliminates Doppler shift automatically.

3.3.2 Resolution and maximum values

3.3.2.1 Comparison of numerical values

Table 3: Measurement limitations when using a single ramp waveform with sweep bandwidth of $B = 250$ MHz and carrier frequency of $f_c = 24$ GHz. A total of $M = 32$ chirps are slow-time processed.

T [µs]	$T \times M$ [µs]	$R_{\max}$ [m]	ΔR [m]	$V_{\max}$ [m/s]	ΔV [m/s]
125	4000	12.8	0.60	25.0	1.56
250	8000	25.6	0.60	12.5	0.781
500	16000	51.2	0.60	6.25	0.390

Table 4: Measurement limitations when using a triangular waveform with sweep bandwidth of $B = 250$ MHz and carrier frequency of $f_c = 24$ GHz.

$2 \times T$ [µs]	$R_{\max}$ [m]	ΔR [m]	$V_{\max}$ [m/s]	ΔV [m/s]
250	12.8	0.60	534	50.0
500	25.6	0.60	534	25.0
1000	51.2	0.60	534	12.5
16000	820	0.60	534	0.781

Consider a device with same parameters as in previous examples. A carrier frequency of $f_c = 24$ GHz, swept bandwidth $B = 250$ MHz, and a sampling interval of $T_s = 2.925$ µs are assumed. Maximum detectable values and resolutions for target range and radial velocity with a slow-time processed single ramp chirps are presented in Table 3. A range of chirp durations T examined. A total of $M = 32$ chirps are collected for slow-time processing.

It can be seen that as the chirp duration increases, so does the maximum detectable range. This is due to the slope of the ramp decreasing, which results in a lower beat frequency for a specific round trip delay. Nyquist limit based on the sampling interval is therefore reached for a longer round-trip delay. The range resolution can be seen to remain constant and independent of the chirp duration, because it depends on swept bandwidth and speed of light alone.

Conversely, a longer chirp duration results in a lower maximum detectable radial velocity. This is because a longer chirp increases sampling interval of the second set of FFTs. A longer sampling interval will result in a lower detectable Doppler frequency. The resolution of the velocity measurement can in turn be seen to improve as the chirp duration increases.

Maximum detectable values and resolutions for range and radial velocity measurements with a triangular chirp are presented in Table 4. Note that since a triangle consists of two ramp sections with an opposite slope, its full duration is effectively twice of that of a corresponding single ramp chirp.

It can be seen that the maximum detectable range behaves in the same way as it does for a single ramp chirp. This is because the range estimation is practically the same for a triangular chirp as it is for a single ramp chirp. The same applies to the range resolution. The only difference is that to get the same maximum detectable range, a triangular chirp needs to be twice as long as a single ramp chirp.

Main difference between the methods lies in their constraints in terms of radial velocity. The maximum radial velocity with a triangular chirp is extremely high. Note that this value was calculated at $R_{\max}/2$. It will be lower elsewhere, but this should demonstrate that it is unlikely to be a problem. Consider, for example, the triangular chirp of 1000 µs in duration. Even at a distance of $0.1R_{max}$, the maximum radial velocity would be 107 meters per second. For an application where 51.8 meters is a reasonable maximum range, the calculated maximum radial velocity is unlikely to ever be a problem.

3.3.2.2 Analysis

Primary difference between slow-time processed ramp chirps and a triangular chirp are their resolutions and maximum detecable values of radial velocity. When using a triangular chirp, the maximum value is extremely high. This due to Doppler shift being calculated from the same spectrum as the beat frequency. The Doppler frequency resolution is essentially the same as for the beat frequency. This means that the radial velocity resolution is very coarse.

Slow-time processing calculates Doppler frequency with an additional round of FFTs. The sampling interval of the transformed time series along columns of the raw data matrix is effectively PRI of the device. Despite there being relatively few samples on each column, the time series still covers a long duration in time. Due to this, it has a high resolution but low maximum value.

Similarly to the maximum detectable value for radial velocity, its resolution also appears to somewhat differ between the waveforms. From Table 4 it can be seen that even though the maximum value remains constant for all chirp durations, its resolution improves for a longer chirp. This is in line with Equation (42), implying

that the resolution is determined by the chirp duration T.

The smallest detectable Doppler frequency can be though of as the shortest period that can fit into the sampled time interval. As was noted earlier, this appears to be quite an unforgiving limitation. A triangular chirp needs to be quite long to have a resolution equivalent to a slow-time processed set of single ramp chirps.

A more careful examination of the relation between chirp duration and the radial velocity resolution reveals that what actually matters is the full duration of time spent sampling a signal. The radial velocity resolution of slow-time processing is determined by total duration of the time series along columns of the raw data matrix. For a triangular chirp, it is determined by the duration of the individual ramps.

From Table 3 and Table 4 it can be seen that a triangular chirp with 16000 µs total duration has an equivalent radial velocity resolution to slow-time processed chirps with total duration of 8000 µs.

A set of slow-time processed single ramp chirps can yield a good radial velocity resolution. A short chirp duration will translate to a short maximum range. Both can be improved with a longer chirp duration, but this will decrease the maximum radial velocity. A single triangular chirp will have the same maximum range as one single ramp chirp of the slow-time processed set, as the range estimation is the same for them. The maximum radial velocity is very high, but dependent on range of the target. The radial velocity resolution appears to be very coarse for short triangular chirps, but can be improved with longer duration.

So far we have only considered processing signals as they were sampled. As was mentioned before, the radial velocity resolution of both methods is dependent on FFT length. It was stated that the resolution can be improved by increasing the length of the FFT with a higher sampling rate. It is possible to improve resolution of the FFT by artificially increasing number of samples by zero padding the signal.

3.4 Zero padding

Zero padding data has found multiple uses across disciplines. Some of these applications include equalizing data packet size [73], and reducing inter-symbol interference [74] in wireless communications. More notably, zero padding has been implemented as part of an interpolation algorithm in computational electromagnetics [75]. This is especially relevant, as the proposed interpolator uses FFT.

Zero padded FFT has been successfully implemented for FMCW radars, both in analysis of phase [57, 55] and frequency [76, 43, 77]. An increased accuracy in range estimation has been demonstrated, but literature on the effect of zero padding on estimated radial velocity is lacking.

The interpolation of the frequency spectrum for a more accurate Doppler frequency estimation has been studied earlier [78], but only for slow-time processing. Furthermore, the Newton interpolation of the spectrum was used rather than zero padding the FFT. It should also be noted that even though a better accuracy was reported, this does not solve the problem of relatively low maximum value of radial velocity pointed out earlier.

The next several pages will be dedicated to demonstrating how zero padding affects accuracy and resolution of an FFT. This will be done using a numerical example using MATLAB and its built-in FFT function.

3.4.1 Signal zero padding and FFT resolution

Zero padding a time series representing a sampled signal will now be outlined. It was shown earlier that when estimating radial velocity with a triangular chirp, the resolution is inversely proportional to the duration of an individual ramp section. This was shown to result in a very coarse resolution. We will now examine how the accuracy of an FFT can be greatly improved through zero padding the signal.

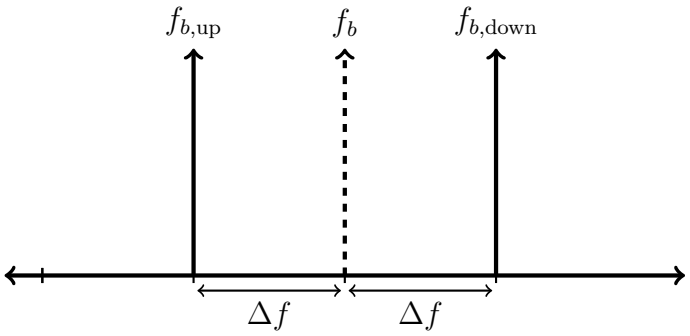

Figure 10: The smallest detectable effect of a positive Doppler shift on up and down ramp sections of a triangular chirp.

Consider the source of radial velocity resolution for measurements with a triangular chirp. The Doppler shift of the returned signal causes up and down ramp section beat frequencies to shift apart. It is clear that the smallest detectable difference between them is one frequency resolution of the FFT. This is illustrated in Figure 10.

Consider now a symmetric triangular chirp with a total duration of $2 \times T$. The signal is sampled with a sampling interval of T_s, so that

$$MT_s = 2T. \tag{44}$$

Note that for purposes of clarity, M has been substituted to denote the length of a time series over N. To analyse the time series separately, they are split into two

equally long parts,

$$0,\ T_s,\ 2T_s\ ,\ldots,\ (M_{\text{up}}-1)T_s, \tag{45}$$

$$M_{\text{up}}T_s,\ldots,\ (M_{\text{up}}+M_{\text{down}}-1)T_s. \tag{46}$$

This implies that

$$M_{\text{up}} = M_{\text{down}} = \frac{M}{2} = \frac{T}{T_s}. \tag{47}$$

Performing an FFT on the two time series results in the frequency resolutions of

$$\Delta f_{\text{up}} = \frac{1}{T_s M_{\text{up}}} = \frac{2}{T_s M} \tag{48}$$

$$\Delta f_{\text{down}} = \frac{1}{T_s M_{\text{down}}} = \frac{2}{T_s M}. \tag{49}$$

Assuming entire chirp duration is sampled, the number of samples is approximately $M = T/T_s$. Substituting this, we get an FFT resolution

$$\Delta f_{\text{up}} = \Delta f_{\text{down}} = \frac{2}{T}. \tag{50}$$

This is obviously twice the resolution of an FFT without splitting the time series into two. Inserting one such FFT resolution into the formula for radial velocity (eq. (14)), we get

$$\Delta V = \frac{c}{2f_c T}. \tag{51}$$

This seems to suggest that previous publications have used an FFT on the full time series rather than splitting it. This makes sense, as the resolution is twice as high than if the series were analysed separately. However, this changes with introduction of zero padding.

Without adding any new actual samples, it is possible to artificially lengthen a time series by padding it with zeroes. A vector of zeroes is simply added to end of a time series, resulting in

$$\underbrace{\overbrace{u_m(t'=0),\ u_m(T_s),\ u_m(2T_s),\ldots,\ u_m(M_{\text{up}}T_s)}^{\text{Sampled up section}},\ \overbrace{0,\ldots,0}^{\text{Zero padding}}}_{M_{\text{up}}+M_{\text{pad}}=2^N} \tag{52}$$

$$\underbrace{\overbrace{u_m(t'=0),\ u_m(T_s),\ u_m(2T_s),\ldots,\ u_m(M_{\text{down}}T_s)}^{\text{Sampled down section}},\ \overbrace{0,\ldots,0}^{\text{Zero padding}}}_{M_{\text{down}}+M_{\text{pad}}=2^N} \tag{53}$$

The time series are padded with zeroes up to some much higher length than originally. Due to simplicity of the implementation, we shall consider padded lengths in powers of two. The built-in FFT function of MATLAB is based on the FFTW algorithm. FFT algorithms are generally optimized for arrays with length in powers of two or small prime numbers for maximum efficiency. [79, 80]

After zero padding, resolution of the FFT is

$$\Delta f_{\text{up}} = \frac{1}{T_s(M_{\text{up}} + M_{\text{pad}})} = \frac{1}{T_s 2^N}, \tag{54}$$

$$\Delta f_{\text{down}} = \frac{1}{T_s(M_{\text{down}} + M_{\text{pad}})} = \frac{1}{T_s 2^N}. \tag{55}$$

Given a high enough N, frequency resolution can be brought down to an extremely low level. A longer padding will increase FFT computation time, so it is worth considering how much accuracy is actually needed.

3.4.1.1 Two frequency components in one time series

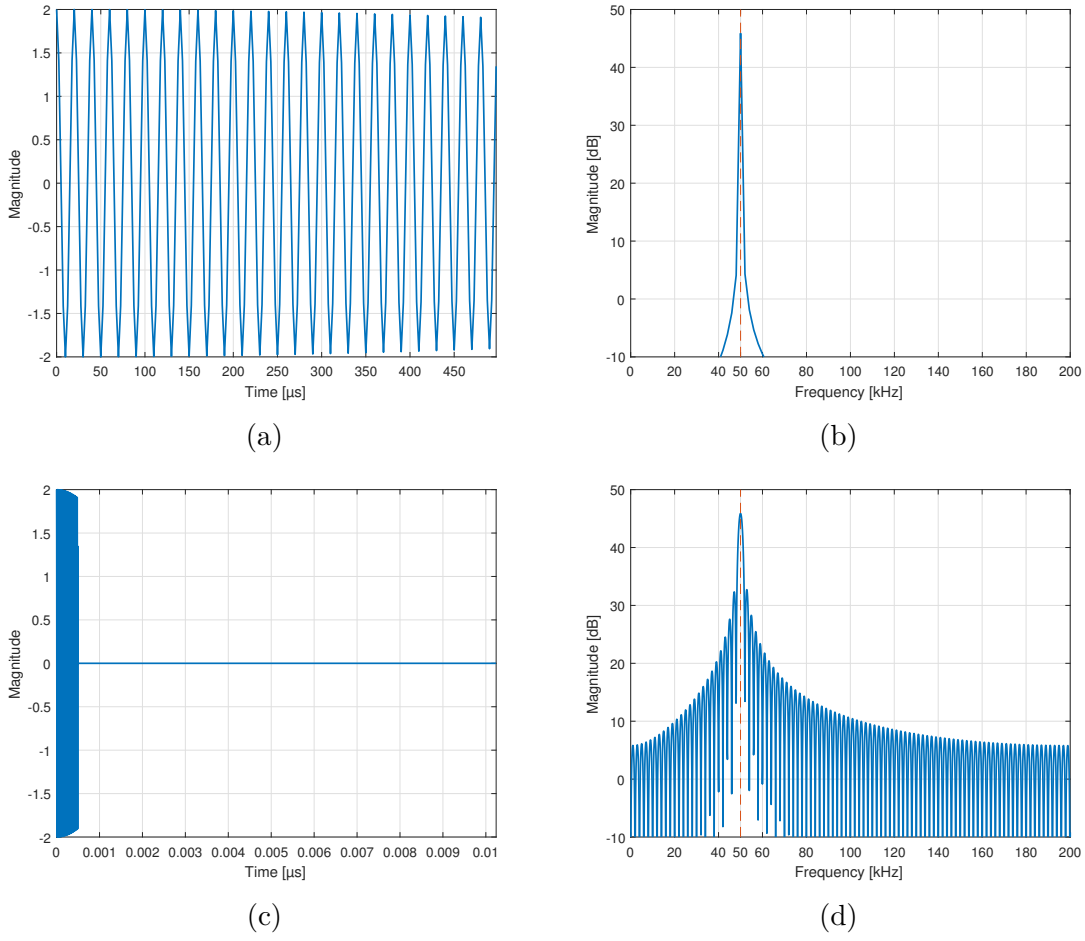

Figure 11: Effect of zero padding on FFT. Unpadded time series (a) and its FFT (b), along with a padded time series (c) and its FFT (d).

Table 5: Number of samples and the corresponding frequency resolution for the unpadded and padded time series.

	Samples	Δf [Hz]
Unpadded	200	2000
Padded	2^{12}	97.7

Let us now examine how zero padding affects FFT in practice. Consider a $T = 500$ µs long signal sampled with an interval of $T_s = 2.5$ µs. The signal is therefore represented by a time series with $M = 200$ samples. The corresponding frequency resolution is 2000 Hz. These values are specified in Table 5.

The signal contains two sinusoidal waves with frequencies very close to each other. It can be written as

$$u(t) = \cos(2\pi(f_1 + f_2)t) + \cos(2\pi(f_1 - f_2)t), \tag{56}$$

where we have chosen the convenient frequencies of $f_1 = 25 \times \Delta f = 50$ kHz, and $f_2 = 0.05 \times \Delta f = 100$ Hz.

The resulting time series is illustrated in Figure 11a, and the resulting FFT in Figure 11b. The two frequency components are 200 Hz apart. The frequency resolution without padding is too coarse to distinguish between the two frequencies.

A zero padding is added to the time series. A generous padding up to $2^{12} = 4\,069$ is chosen. Corresponding resolution can be calculated to be approximately 97.7 Hz. These values can also be seen in Table 5. Padded time series is illustrated in Figure 11c, and the corresponding FFT in Figure 11d.

Despite the zero padded FFT resolution being smaller than difference between the two frequency components, only one peak can still be seen in the spectrum. This demonstrates that a zero padded spectrum is essentially just an interpolation of an unpadded spectrum. If frequency components cannot be told apart in the unpadded spectrum, zero padding will not make them distinguishable either. Relationship between the frequency difference and the unpadded FFT resolution warrants further investigation.

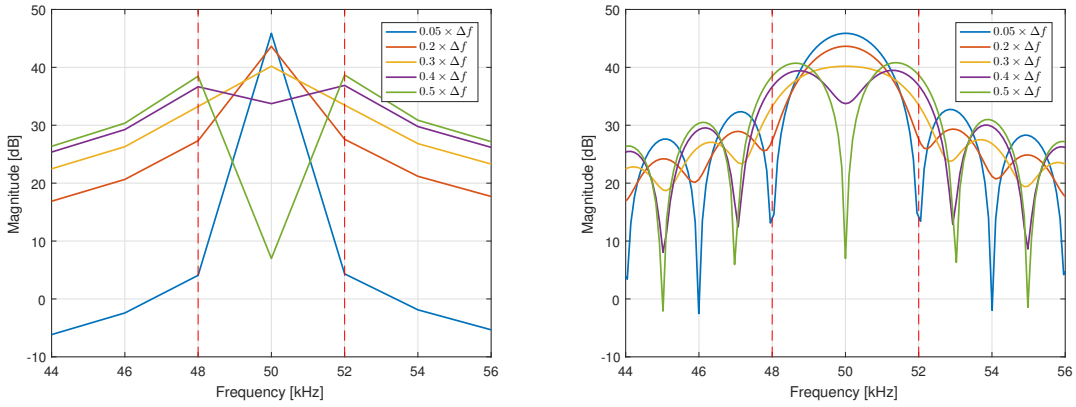

(a) (b)

Figure 12: Effect of f_2 on the (a) unpadded and (b) padded FFT. Legend specifies value of f_2 as a fraction of unpadded FFT resolution.

Effect of frequency difference of the unpadded and padded FFT is illustrated in Figure 12. The second frequency component f_2 is varied from the original $0.05 \times \Delta f$ to $0.5 \times \Delta f$. In Figure 12a, the magnitude of the unpadded FFT is illustrated for each value of f_2.

Increasing f_2 causes two different FFT peaks to emerge and drift apart. The peaks are not distinguishable from each other until difference between them is at least approximately one unpadded FFT resolution. In the padded FFT illustrated in Figure 12b a similar behavior can be observed, although more accurately. The peaks begin drifting apart as the frequency difference increases.

For the smallest f_2, it can be seen that the two frequencies have merged into one lobe. Its width is approximately two unpadded FFT resolutions, or 4 kHz. The same behavior can be observed until the second frequency component is $0.4 \times \Delta f$, when two peaks appear. However, not until the frequency is 0.5 of the original resolution does a clear null appear between the peaks, and they can reliable be identified as two separate lobes.

It would seem that if the unpadded FFT is not sufficient in resolution, zero padding can't be used to distinguish frequencies that are closer to each other than the original FFT resolution.

Since fractions of the FFT resolution were used as frequencies, these observations will apply to any other signal duration consisting of any two frequencies. Similarly, this would apply to three distinct frequencies as well. Frequency components less than one unpadded FFT resolution away from each other are indistinguishable.

From Figure 12b it can also be seen that even though for $f_2 = 0.5 \times \Delta f$ difference between the two peaks should be $2 \times 0.5 \times \Delta f = \Delta f = 2$ kHz, it actually

appears to be slightly more. This could be expected. The resulting spectrum is simply the sum of the individual spectra of each frequency component in the signal. Because of discrete sampling, they are not the familiar impulse function of a continuous sinusoidal wave. The effect does not seem to be very significant, and does not warrant further discussion.

3.4.1.2 Two frequency components in two separate time series

In the previous example, it was demonstrated that two separate frequency components are indistinguishable if their difference is less than the original, unpadded FFT resolution. However, the radial velocity estimation with a triangular chirp is based on the separate analysis of the up and down ramp sections. We will now examine the effect of zero padding when attempting to distinguish between two frequency components in separate time series. This is done with a simple MATLAB simulation of a triangular chirp.

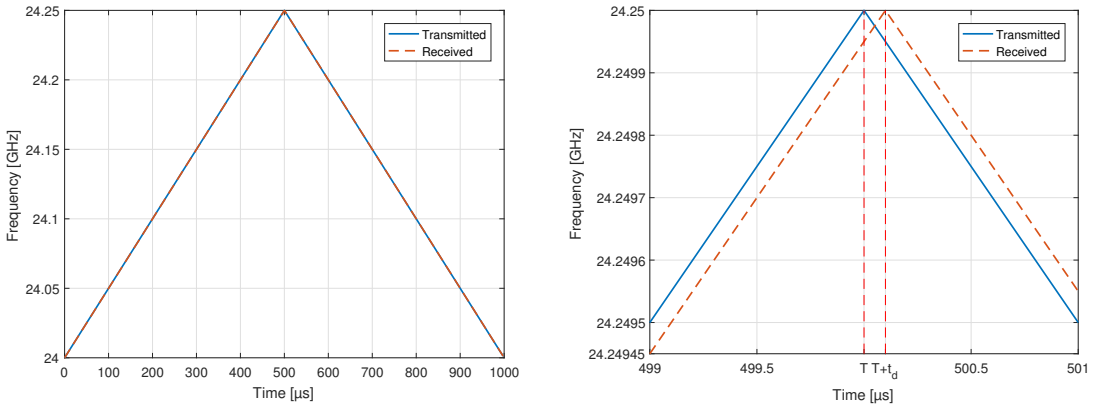

(a) (b)

Figure 13: (a) Frequencies of transmitted and received triangular chirps as a function of time. (b) A zoomed version displaying frequency difference due to round trip delay more clearly.

Assume a triangular chirp with up and down section ramp durations of $T = 500$ µs, for a total duration of $2 \times T = 1000$ µs. The frequency of the chirp is swept from a carrier frequency f_c of 24 GHz to 24.25 GHz, resulting in a bandwidth of $B = 250$ MHz. Similarly to the previous example, we assume that the signal is sampled with an interval of 2.5 µs. The triangular chirp is represented with a time series consisting of $M = 400$ samples.

Transmitted and received triangular chirps are analyzed, which means that this example also somewhat demonstrates how the FMCW radar works. In Figure 13a illustrates the transmitted and received triangular chirps. A zoomed version of the situation is illustrated in Figure 13b. The effect of the round trip delay is clear. The

delay has been chosen so that the frequency difference between the transmitted and received chirps is $f_1 = 50$ kHz, corresponding to a round-trip delay of 100 ns.

The transmitted signal is described as a sinusoidal wave with a linearly changing frequency,

$$u_t(t) = \cos\Big(2\pi f_{\mathrm{mod}}(t)t\Big), \tag{57}$$

where f_{mod} is a triangular function. Conversely, received signal has its frequency delayed by the round-trip delay,

$$u_r(t) = \cos\Big(2\pi(f_{\mathrm{mod}}(t - t_d) + f_2)t\Big). \tag{58}$$

An additional frequency shift of $f_2 = 100$ Hz has been added to the signal. In practice, this corresponds to a Doppler shift due to a moving target.

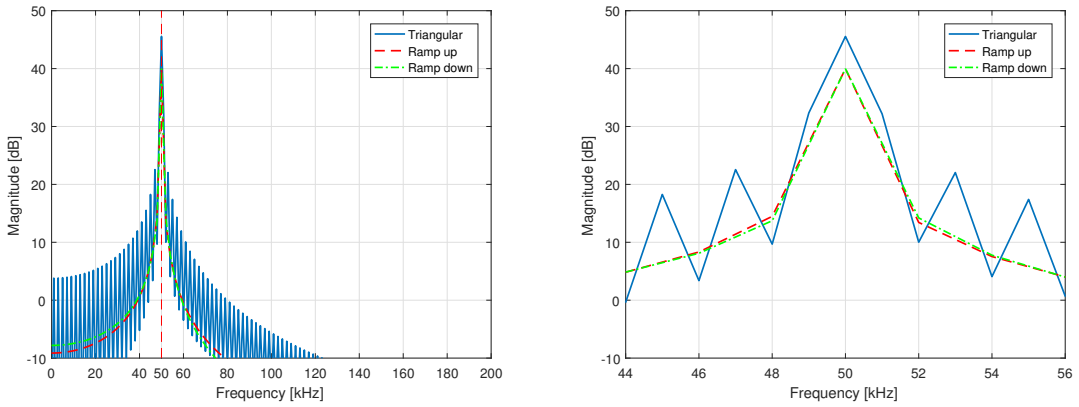

(a) (b)

Figure 14: (a) The resulting FFT of the full time series (Triangular in legend), and both up and down ramp sections when analyzed separately. (b) A zoomed version around the apparent peak frequency.

Table 6: Numbers of samples for unpadded and padded full triangular time series and the separate up and down ramp sections, along with the corresponding frequency resolutions.

	Triangular		Ramp up		Ramp down	
Samples	400	2^{12}	200	2^{12}	200	2^{12}
Δf [Hz]	1000	97.7	2000	97.7	2000	97.7

Up and down ramp section of the triangular chirp are now analyzed together and separately. The number of samples and the resulting frequency resolution for each

analyzed time series is specified in Table 6. The label triangular refers to the entire time series, and ramp up and down to the respective sections separately.

First, we analyse the entire time series of the sampled triangular chirp. The resulting FFT resolution is 1 kHz. The full series is then broken down into two separate time series of equal length. The resulting frequency resolution is 2 kHz. Similarly to the previous example, a generous zero padding up to 2^{12} is considered, bringing the frequency resolution down to 97.7 Hz.

The magnitudes of unpadded FFTs are illustrated in Figure 14a. A zoomed version of the spectrum around the peak is illustrated in Figure 14b. The frequency resolution is too coarse in all cases to detect f_2. However, a very slight shift can be seen between the up and down ramp section spectra. The ramp up section would appear to be shifted slightly to the left, while the down section is shifted slightly to the right. This makes sense, as the up section has a slightly higher frequency than the down section. Since the corresponding magnitudes are so small, and all estimations should be based on apparent FFT peaks, this really isn't useful information. Resolution is simply too coarse to see any difference, even when analysing up and down sections separately.

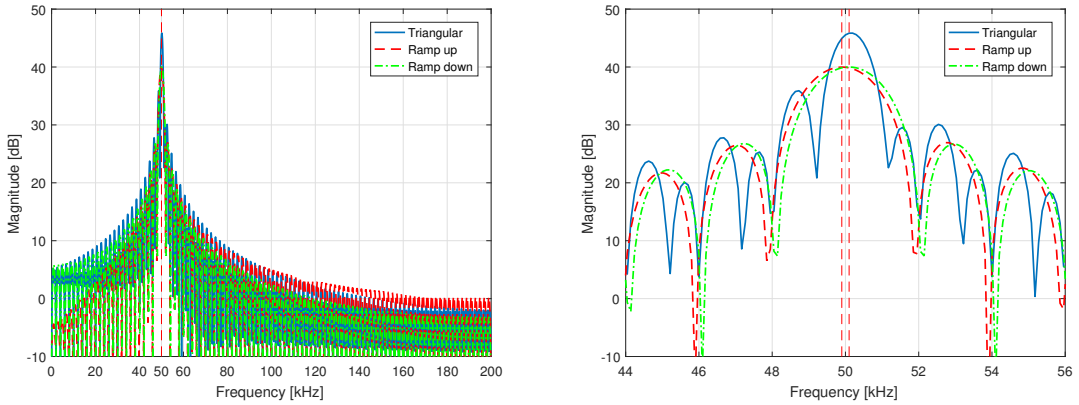

(a) (b)

Figure 15: (a) The resulting FFT of the zero padded full time series (Triangular in legend), and both up and down ramp sections when analyzed separately. (b) A zoomed version around the apparent peak frequency.

The magnitude of the zero padded FFT is illustrated in Figure 15a. An illustration of the spectra when zoomed closer to the frequency peak is shown in Figure 15b. An unexpected behavior of the full triangular time series spectrum can be observed. Its peak appears to have shifted to a slightly higher frequency. This is probably caused by the presence of a non-constant frequency in the time series. The reason and causes behind this shift are no doubt interesting, but largely irrelevant to the work at hand.

True motivation for splitting the original time series into two and analysing them separately can be seen in the difference between up and down ramp section FFT spectra superimposed on Figure 15b. There is now a noticeable difference between the frequency peaks. In fact, since the frequency resolution due to zero padding is 97.7 Hz, the distance between up and down ramp section peaks corresponds to two zero padded FFT bins. The additional frequency component of $f_2 = 100$ Hz is effectively rounded to the nearest integer multiple of the zero padded frequency resolution, or in this case 97.7 Hz.

This clearly demonstrates that as long as FFTs are performed separately, zero padding can be used to find a relatively small frequency difference between two time series. Simply a long enough zero padding is required.

3.4.2 Practical implications

The process of zero padding and its effect on a sampled signal has been presented and evaluated using some simple MATLAB examples. It was discovered that frequency components that are closer than unpadded frequency resolution of the FFT are indistinguishable from each other. This is in line with the assessment that zero padding the signal essentially gives no new information about the number of frequency components, but rather results in an interpolated version of the unpadded FFT.

This observation has the following practical implication when performing measurements with an FMCW radar. Two targets will produce two distinct beat frequencies when the transmitted and received chirps are mixed. However, if these two targets are closer to each other than the range resolution given in Equation (29), they will be indistinguishable from each other. This is due to the effect observed in Figure 12b, where two close frequencies merge into peak. Each lobe produced by a target can in turn be expected to be two unpadded frequency bins wide.

Zero padding the signal smooths the original FFT, allowing position of the peak of an FFT lobe to be found more accurately. This is also the foundation of the next practical implication relating to estimating the Doppler shift with a triangular chirp.

The first example related to range information and target discrimination. This was done with one time series containing two distinct frequencies, which was analogous to two targets in very close proximity to each other. However, the method for estimating the Doppler frequency from a triangular chirp is based on separate analysis of two time series.

As was stated earlier, two frequency components too close to each other will essentially meld into one lobe in the FFT regardless of the zero padded length. However, if they are in separate time series this no longer is the case. It was also shown that frequency corresponding to the peak of this lobe can be found more accurately with zero padding. Hence, if the frequencies are in two different FFTs, they can be

distinguished very accurately even for a relatively small difference.

4 Device overview

This section provides a brief overview of the radar device used for all of the measurements. The device itself was developed as part of an effort to create a navigation aid for visually impaired. It has been found to be reliable, and has been used in previous research [13, 32]. A simplified block diagram of the radar device will be presented, along with specifications of the key components. Waveforms generated by the radar will also be illustrated and discussed.

4.1 Layout

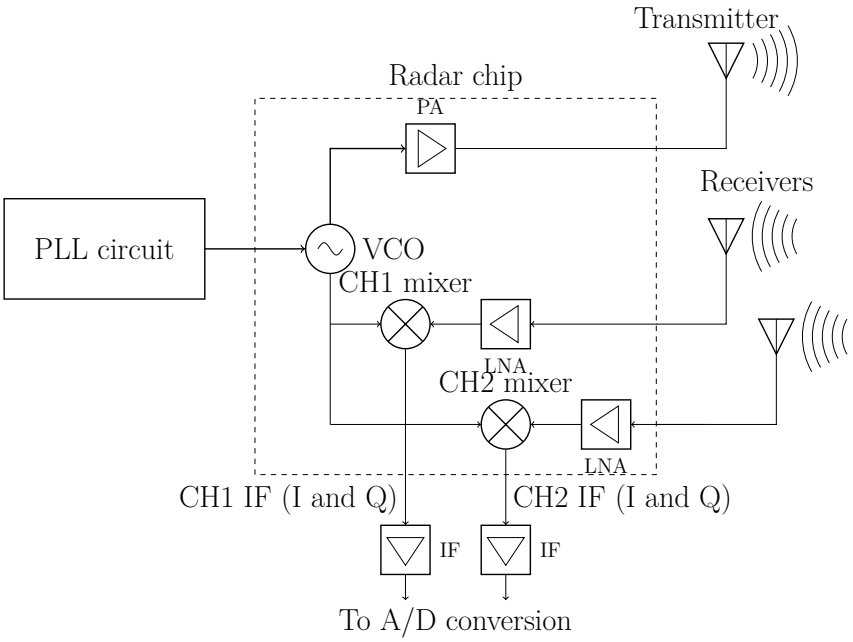

Figure 16: Diagram of the radar device analog components.

A simplified block diagram of the radar device structure is illustrated in Figure 16. A PLL circuit is used to generate a voltage waveform, which in turn drives a voltage controlled oscillator (VCO). Voltage from the PLL is used to sweep a given bandwidth. The signal is then radiated by a transmitting antenna.

The radar device has been designed to operate with two identical receivers. This way, interferometry technique [7, 81] can be used to approximate the direction of arrival of a signal. This will not be considered in this work, so the extra data will instead be used to lower the noise floor of the measurements.

Amplifiers are used for both of the receive channels to compensate for power attenuation due to the quartic term $1/R^4$ in the received signal. Received signals are then mixed with the transmitted signals, resulting in a round trip delay dependent beat frequency. In phase and quadrature components (I/Q data) [41] of the mixed signals are forwarded to A/D conversion and signal processing.

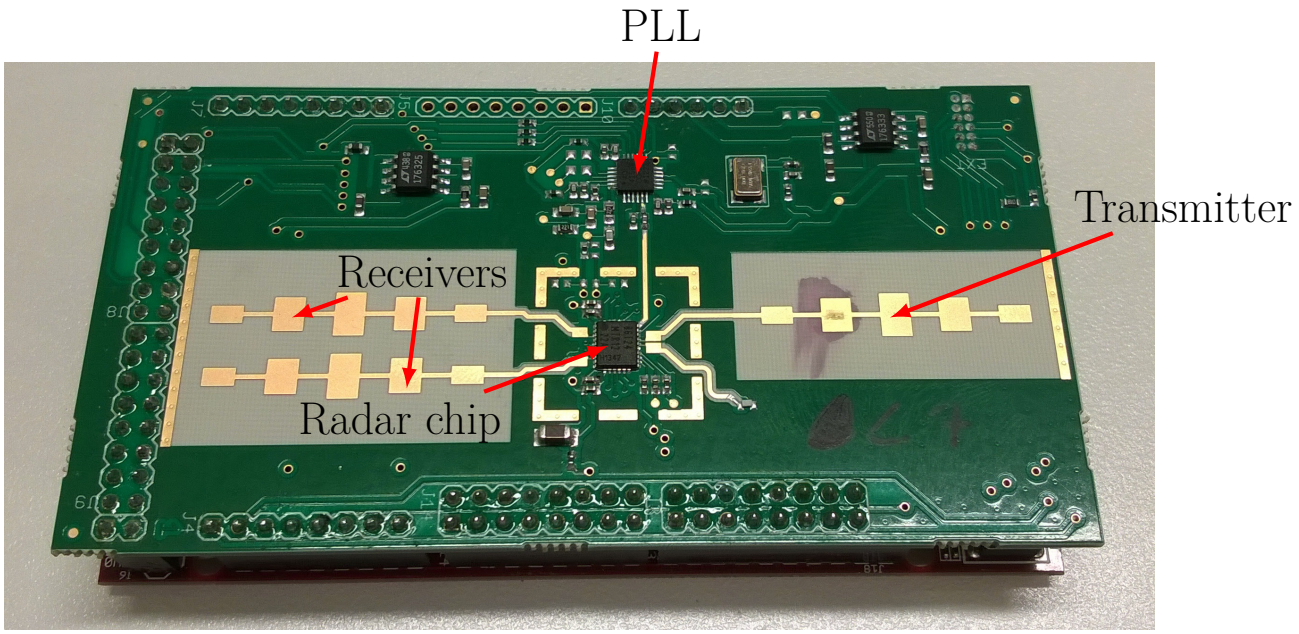

Figure 17: A top view of the radar device. Principal analog devices highlighted.

A top view of the radar device used in all measurements is presented in Figure 17. Identical patch antennas have been used for both reception and transmission. The phase difference between signals from the two receivers can be used to estimate the direction of arrival of a signal. Since there are only two receivers, this can be done only in a plane that is orthogonal to them.

Device	Radar chip	PLL circuit
Model	BGT24MTR12	ADF4158
Notes	Infineon [82]	Analog Devices [83]

Device	Microcontroller	Reception and transmission
Model	PIC32MX795F512L	Patch antennas
Notes	Microchip Technology[84]	Optimized for 24-24.25 GHz (ISM) band

Table 7: Principal components of the radar device.

Principal components used in the radar device are illustrated in Table 7. An Analog Devices ADF4158 [83] is chosen as the waveform synthesizer. It is capable of being

programmed to generate simple sawtooth, ramp, and triangular voltage waveforms. Duration, delayed start, and number of steps to complete the voltage sweep are all programmable features that must be considered.

An Infineon BGT24MTR12 radar chip [82] is used as the component responsible for generating, transmitting, and receiving the radar chirp. The component contains a VCO that is driven by the PLL. It is capable of handling two sets of receivers and transmitters. For this purpose, two transmitters and one receiver was used. Circuitry that mixes the transmitted and received signals, and outputs the resulting I/Q data is also included.

Transmitter and receivers of the radar device are planar patch antennas on top of a dielectric substrate. They are illustrated in Figure 17.

A Microchip Technology microcontroller model PIC32MX795F512L [84] is used to control the entire device. It is responsible for controlling register values of the other components, A/D converters, and other tasks vital for the device's operation. The device can be connected to a desktop computer and programmed using a PICkit programmer of the same manufacturer.

4.2 Generated triangular waveform

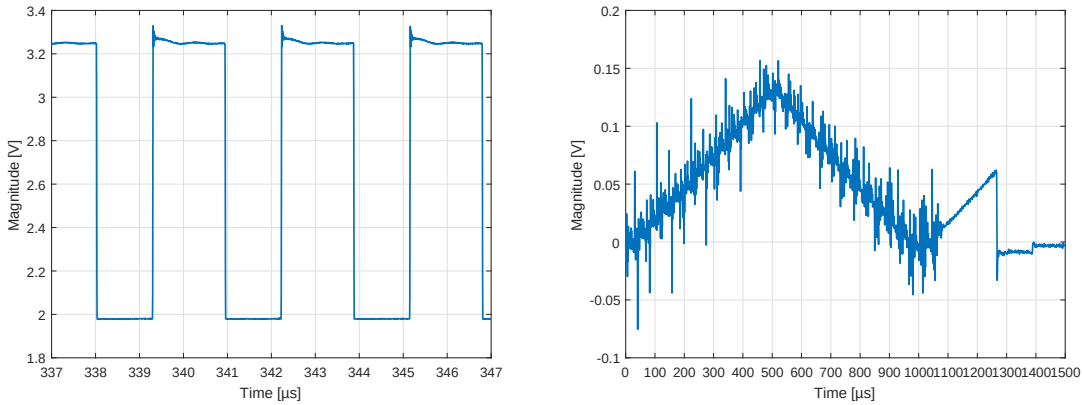

(a) (b)

Figure 18: (a) The chip select waveform of the microcontroller, and (b) a 1000 µs long triangular voltage waveform fed into the radar chip.

Some waveforms generated in the radar device are illustrated in Figure 18. In earlier sections, importance of the sampling interval of the time series analyzed with FFT has been underlined. Voltage controlling the A/D sampling is illustrated in Figure 18a. A period of the square wave corresponds to one A/D sampling interval. From this figure it can be determined that one period of the square wave and therefore sampling interval of the device is approximately 2.925 µs.

A snapshot of a triangular waveform generated by the PLL is illustrated in Figure 18b. The measurement was performed at voltage input of the radar chip, after it had been through a filter and some circuitry. The waveform consists of two linear ramps with opposite slopes, and has a total duration of 1000 µs. Sampled period of the waveform corresponds to the section with higher noise. For good measure, the sampled period is chosen as slightly longer than the actual waveform. This is to ensure that both up and down ramp sections are fully sampled.

It should be noted that only a continuous triangular waveform can be generated with the chosen PLL circuit. A single burst is not an option. This is evident in the waveform's behavior after the sampled interval ends. Due to delays in controlling register values of the different components, a new waveform is started before the PLL is switched off.

Before the PLL's voltage is used to drive the VCO, it is fed through a smoothing filter. This ensures cleaner and more consistent transmitted signal.

5 Measurements

This section presents actual measurements performed with the radar device. Measurements were carried out in an anechoic chamber, and a generic office environment. Setups and locations of the measurements will be presented and discussed. Reference equipment needed during the measurements will also be briefly presented.

Practical implementation of the signal processing methods presented in earlier sections will also be discussed and demonstrated using a snapshot of one measured data set.

The focus of this section is on data acquired during measurements in the anechoic chamber. The results will be presented in a series of figures and discussed in their corresponding subsections. For good measure, similar measurements were also carried out in a more realistic setting. Using some representative results, it will be demonstrated that the method described in this work is valid and robust in more cluttered environments as well. It does not rely on a ideal environment, such as an anechoic chamber.

5.1 Reference equipment

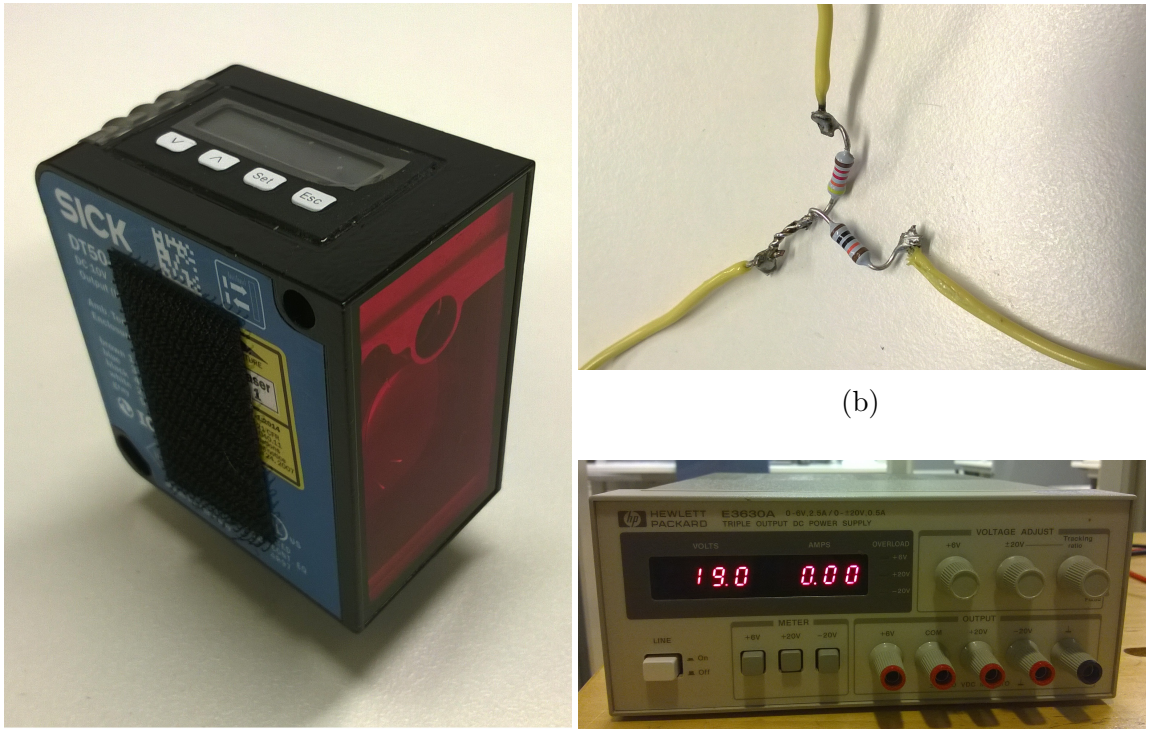

(a) (b) (c)

Figure 19: Equipment used during the measurements. (a) DT50 distance sensor used as a reference, (b) a simple voltage divider constructed to scale output voltage of DT50 down, and (c) the power supply used by the sensor.

To assess the accuracy of range and radial velocity estimation with a triangular chirp, a DT50-2 model mid range distance laser sensor [85] was used. The device will simply be referred to as DT50 from here on. To power the sensor, a Hewlett Packard power supply was used to provide an operating voltage of approximately 20 volts DC. The supply also provided a common ground for the measurement setup. The devices are illustrated in Figure 19.

The DT50 sensor measured distance to a point illuminated by a laser point to an accuracy of ± 0.7 millimeters. The measuring range of the sensor was up to 10 meters on an absorbing target and up to 30 meters on a well reflecting target. The sensor output was chosen as a DC voltage between 0 and 10 volts for a programmable range. An A/D converter built in to the microcontroller of the radar device was used to sample the voltage before the transmission of each sweep. Because the operating range of the A/D converter was ± 3.3 volts, a simple voltage divider was constructed to scale down output voltage of the DT50 sensor.

Resistors with values of 100 kΩ and 43.2 kΩ were soldered together with short wires for safely connecting them. When the smaller resistance was connected to

ground and the larger to the DT50 output, voltage over the smaller resistance was scaled down to approximately one third. Output voltage could then be sampled using the built in A/D converter.

5.2 Estimating range and radial velocity of a target from sampled I/Q data

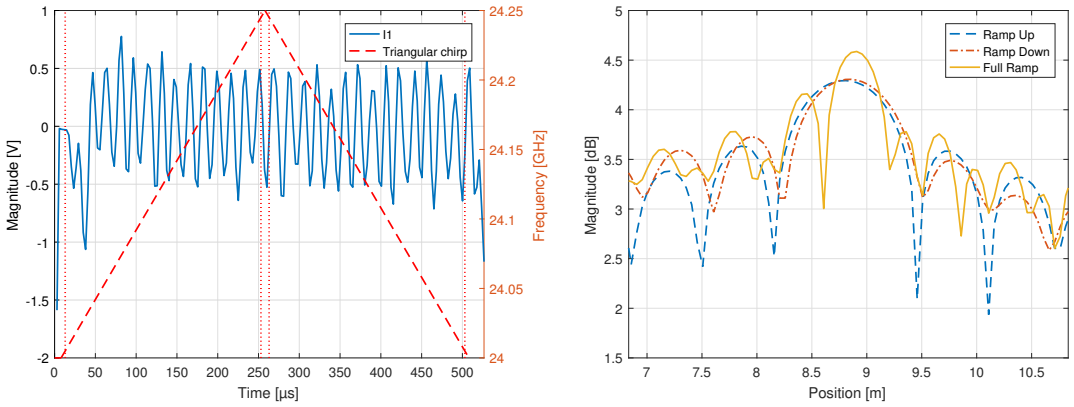

(a) (b)

Figure 20: Snapshot of signal processing. (a) The voltage of the first in phase channel (I1), and the corresponding triangular frequency waveform. (b) FFT of the I1 channel, with full time series (Full ramp), and sections of the time series delimited by dotted red lines (Ramp up and down).

Since the employed radar chip outputs the in-phase and quadrature components from two receivers, we essentially have four separate signals that can be used in detecting a target and estimating its parameters. A snapshot of voltage from one of these channels is illustrated in Figure 20a. A 500 µs triangular chirp is used in the snapshot. The triangular waveform in frequency domain is superimposed on the figure. Its frequency is specified in the right y-axis.

Dotted red lines illustrate which samples are being used in the analysis. A margin of five microseconds is included before and after an up or down ramp section begins. This ensures that the waveform has time to settle, and that a clean sample of the beat frequency is acquired.

Sampling the channels begins at time $t = 0$, but the triangular chirp is programmed to be started only 8 microseconds after this. This means, for example, that analyzed samples of the up ramp lie between 13 and 253 µs. This is done so that the waveform has time to settle to the carrier frequency before beginning the sweep. The waveform is also allowed to continue for a while after the chirp has been completed. This is to ensure that one full triangular chirp is sampled.

Figure 20a illustrates the somewhat periodic nature of the channels. A point of symmetry can be seen near the point in time which corresponds to the tip of the triangle. It can also be seen that the triangular chirp is generated continuously rather than in bursts. Voltage in the channels continues to oscillate even after the triangular chirp has ended. This is because the used hardware does not permit the generation of bursts of triangular chirps. Instead, the PLL briefly begins a new triangular chirp.

	I1	Q1	I2	Q2	Mean
Range [m]	8.83	8.85	8.85	8.81	8.84
Radial velocity [m/s]	1.04	2.09	2.09	0	1.30

Table 8: Range and radial velocity estimated from channels means of the snapshot. I and Q are shorthand for in-phase and quadrature components of the first and second receivers, respectively.

After each sweep has been sampled, an FFT is performed individually on each channel. The result of this is illustrated in Figure 20b. In this example, a zero padding up to 2^{10} was used. Using the resulting frequency resolution and methods presented in earlier sections, the frequency spectrum is converted into range information.

The range to the target is estimated for each channel from the mean of the ramp up and down section peak positions. The Doppler shift due to radial velocity of the target is estimated from the difference between the peaks. These values are specified in Table 8. Actual range and radial velocity of the target is then estimated from a simple mean of the individual channel results.

A further observation can be made from Figure 20b. Graph labelled as Full Ramp in the figure is simply the full time series from Figure 20a. No samples have been dropped. It can be seen that the spectrum has no clear peak where the target should be. As such, no accurate estimations can be made from the full information. It is clear that the full ramp information is not very useful.

Samples are dropped before an individual ramp sections begins and ends. This is done to acquire a clean as possible sample of the beat frequency. A possible explanation for the full time series spectrum not showing a clear peak is that extra frequencies have been introduced to the spectrum. The ramp up and down section peaks are so close that they might somehow interfere with each other. Similarly, extra frequencies may have been introduced from the beginning, end, and halfway points of the triangular waveform. Reader should refer back to the section on waveforms to get a better idea.

5.3 Anechoic chamber

The first set of measurements were carried out in an anechoic chamber operated by VTT. The chamber is located at Otakaari 7, Otaniemi. Its measurements were $12 \times 12 \times 17$ m^3 [86]. The site was chosen due to its size, ease of access, and known high quality.

The measurements were performed in an anechoic chamber in general to firstly minimize any possible outside interference, multiple reflections and multi-path propagation, and the presence of other targets which might adversely affect the measurement results.

The purpose of these measurements was to demonstrate the accuracy of the proposed method, and to highlight the relevant phenomena as clearly as possible. A corner reflector was used for the same reasons. Hence, any sources of noise and errors were sought to be minimized.

5.3.1 Moving target

5.3.1.1 Measurement setup

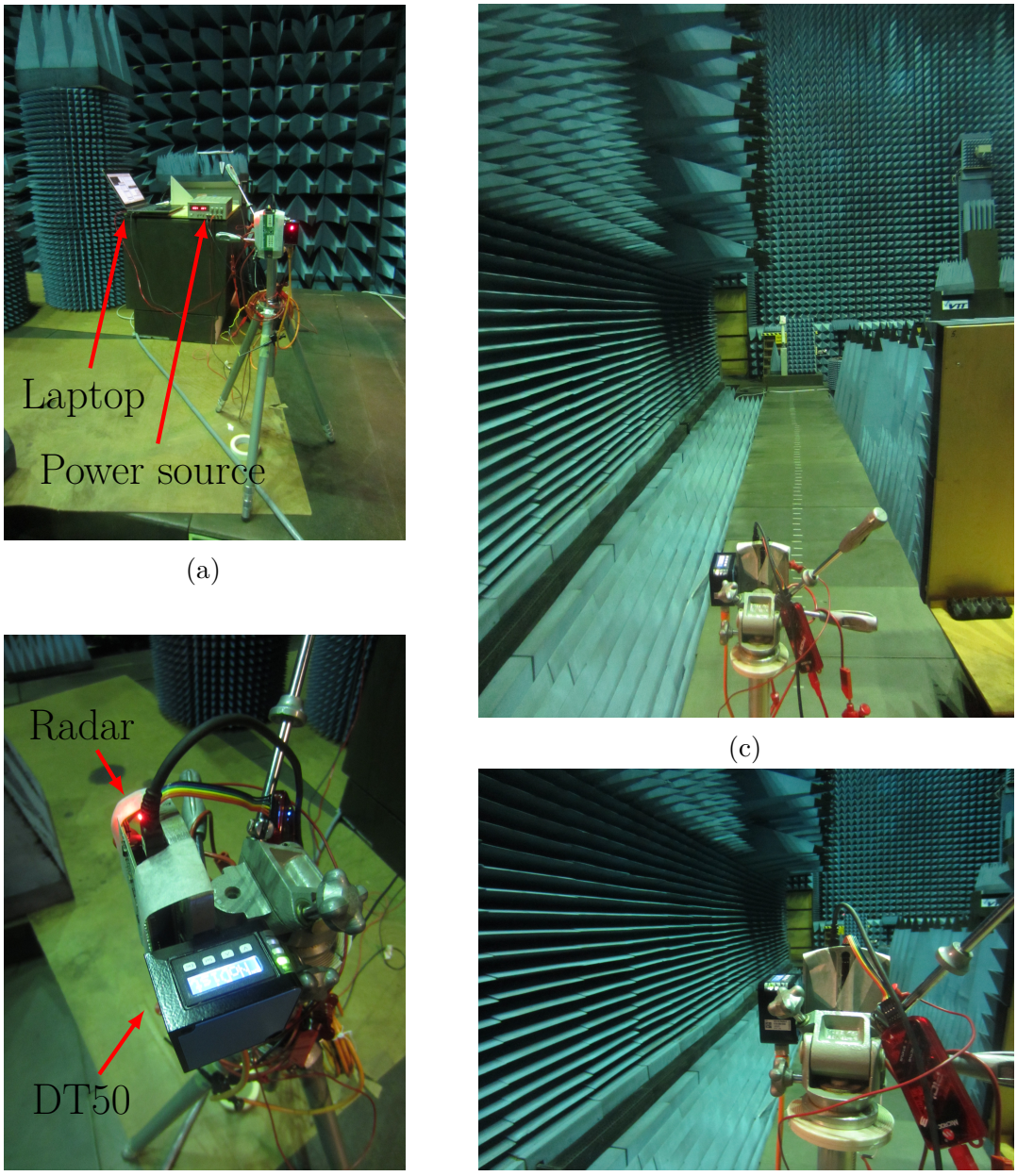

(a)

(c)

(b)

(d)

Figure 21: Measurement setup in the anechoic chamber. (a) A front view of the setup. (b) A top view of the setup. (c) View down the walkway used as a testing range. (d) A rear view of the setup.

The setup of the first measurement is illustrated in Figure 21. A frontal view of the measurement setup is shown in Figure 21a with power source and laptop highlighted. The laptop is connected to the radar through a PICkit used to program the microcontroller of the radar device, and an UART link to import the measured data to the laptop. The radar device and the DT50 sensor are mounted on a tripod at the start of a walkway used as the testing range.

Figure 21b shows a top view of the setup. The radar device is securely attached to the front of the tripod using a generic adhesive tape. Next to it is the DT50, which has been secured to the tripod using a velcro strip. Visible are also the multicoloured wires used to connect the radar to the PICkit, and the black cable used for the UART link.

Figure 21c shows a view down the walkway that connects the back of the anechoic chamber to the front with a door used to access it. This walkway was used as a testing range, and was approximately 10 meters in length.

Finally, a rear view of the measurement setup can be seen in Figure 21d. The PICkit is more visible, as is the orange cable containing wires for the DT50 output and input. Its ground was connected to the common ground provided from the power source, and the DC voltage output to the A/D converted of the radar device microchip.

The measurement procedure was simple. A test subject stood in the opposite end of the walkway holding a corner reflector. The laptop was used to order the radar to begin transmitting and sending data over to the laptop. The received data was saved in text files, and later accessed with MATLAB. Once the radar had begun to transmit, the test subject walked briskly until approximately one meter away from the radar device. The subject then turned around, and walked back to the opposite end of the walkway, while maintaining the orientation of the corner reflector so that it continued to face the radar device.

Since the DT50 measured the distance to a point illuminated by the laser, some issues were encountered. Sometimes the laser dot missed the test subject, rendering the measurement useless. The results were thus forced to be discarded. Three triangular chirp durations were used, and each measurement was repeated five times. The most representative results are presented in the following subsections.

Triangular chirp duration $2 \times T$ [µs]	250	500	1000
Samples	93	180	350
Time step [s]	0.113	0.137	0.193

Table 9: Average time step between each chirp due to the delay introduced by the UART link.

Since the measured data had to be imported to the laptop for analysis, a relatively long delay was introduced between each chirp. For each chirp, the voltage given

by the DT50 was first measured. It was then sent over the UART link and saved into a text file. After this, the chirp was triggered and sampled. Once the sampling was finished, the data was seen over the UART link. The UART link was found to be very slow, but still fast enough for it not to have an adverse effect on the measurement. The radial velocities involved in the measurements were clearly small enough for the time step to be small enough as well. Time steps due to the UART link delay are specified in Table 9.

5.3.1.2 Results

5.3.1.2.1 250 microseconds

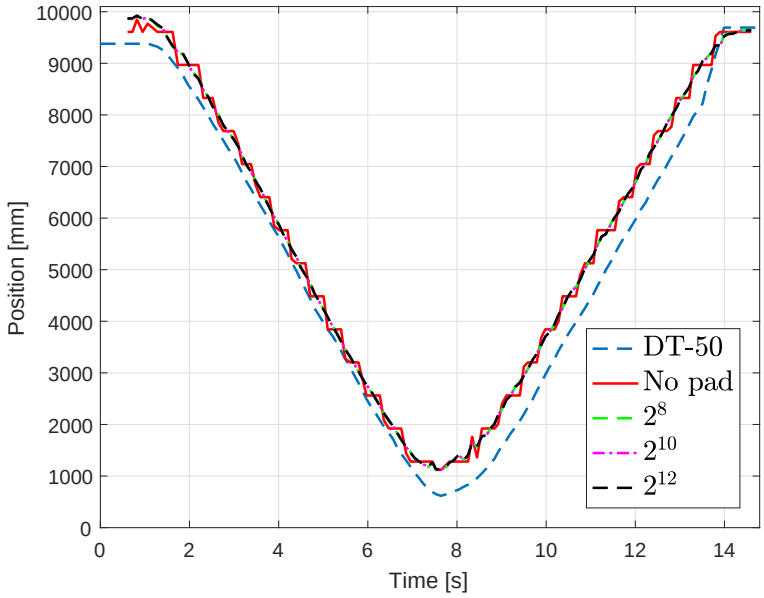

Figure 22: Range estimated from data acquired with a triangular chirp $2 \times T = 250$ µs in duration. Zero padded lengths specified in legend.

Position and radial velocity of a walking target were estimated using the channel mean method specified earlier. Range information acquired with the reference device DT50 is illustrated with the dashed blue line in Figure 22. A solid red line is used to illustrate an unpadded range estimation, and the rest are for different zero padded lengths. In both results, a target can be seen to approach the measurement setup from approximately 9.5 meters to 0.5 meters and back, over the course of approximately 14 seconds.

The unpadded range estimation can be seen to follow the trend of the reference measurement well. However, since frequency resolution of the FFT is so poor, the graph can be seen to proceed in steps. These steps approximately correspond to the

unpadded range resolution of 0.6 meters, but not exactly. This is due to some of the samples being dropped right before the beginning and end of the ramp sections. Increasing zero padding can be seen to have a significantly smoothing effect even with a relatively short padding of 2^8. After this, increased padding can be seen to have a very diminished effect. There appears to be no clear difference between paddings of 2^{10} and 2^{12}.

Despite the increased zero padding, a systematic error appears to persist in the results. There appears to be a somewhat constant difference between the reference data and estimated range. The source of this is not known, but can be speculated on later. The same effect can be observed in all measurements.

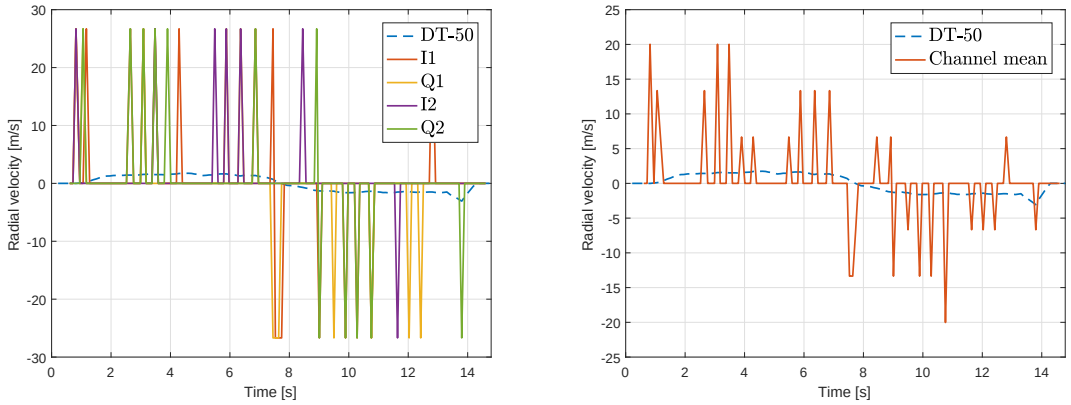

(a) (b)

Figure 23: Radial velocity estimated from unpadded individual channels (a), and the channel mean (b). Triangular chirp duration $2 \times T = 250$ µs.

In Figure 23, the radial velocity of the walking target is estimated from raw unpadded data. Even though all relevant information is included in the raw data, it is difficult to interpret. The above figure demonstrates this. Velocity calculated from individual channels can be detected in jumps of approximately 26.7 meters per second. This is what could be expected, since the smallest shift that can be detected between the up and down ramp section FFT peaks is one frequency resolution. After dropping samples, the unpadded time series are both 40 samples long. With a sampling period of $T_s = 2.925$ µs, this results in an approximate frequency resolution $\Delta f \approx 8.55$ kHz. Inserting this into Equation (14) results in the observed radial velocity jump.

Radial velocity estimated from unpadded data appears to be useless in any accurate estimations of target radial velocity. Taking the channel mean of the results appears to provide little help. However, the results would still appear to correctly indicate whether the target is travelling towards or away from the radar. It is interesting that the unpadded range estimation appears to be far more accurate than

unpadded radial velocity estimation.

Due to its obviously low information value, no further radial velocity analysis will be performed on the unpadded data.

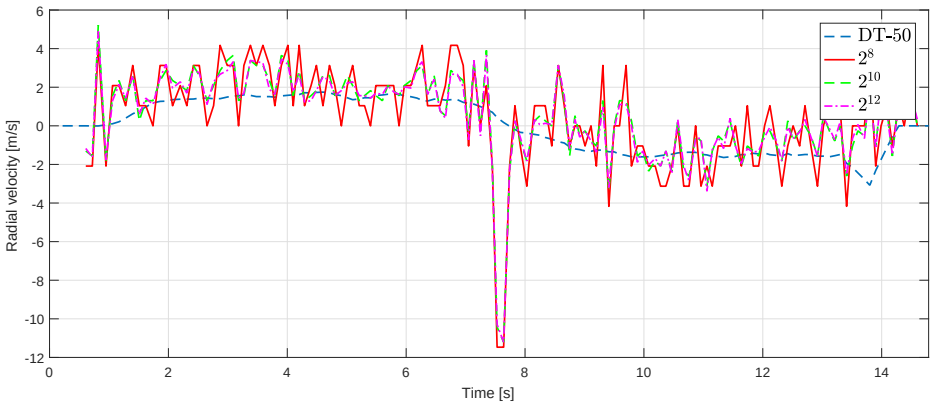

Figure 24: Radial velocity estimated from data acquired with a triangular chirp $2 \times T = 250$ µs in duration. Two results presented.

Effect of zero padding on the estimated radial velocity is illustrated in Figure 24. As with the range estimation, a set of different zero paddings are studied. Similarly to the range estimations, it can again be observed that a zero padding to 2^8 greatly improves the results. Without padding, the estimated radial velocity was completely in the wrong magnitude and very discontinuous. Although it would appear that the padded results are still very noisy, they overall seem to indicate the correct direction of movement, and magnitude with some reservations.

Increasing the zero padding has an effect that is similar to the range estimations. The first padding provides the clearest improvement, and the effect is diminished for the rest. When the change from 2^8 to 2^{10} and 2^{12} is compared, it appears that the graph is approaching a set of so called final values. It can also be seen that some extreme errors, especially between 6 and 8 second marks, cannot be corrected using zero padding. Rather, the graph simply approaches some value there as well while retaining a high error.

5.3.1.2.2 500 microseconds

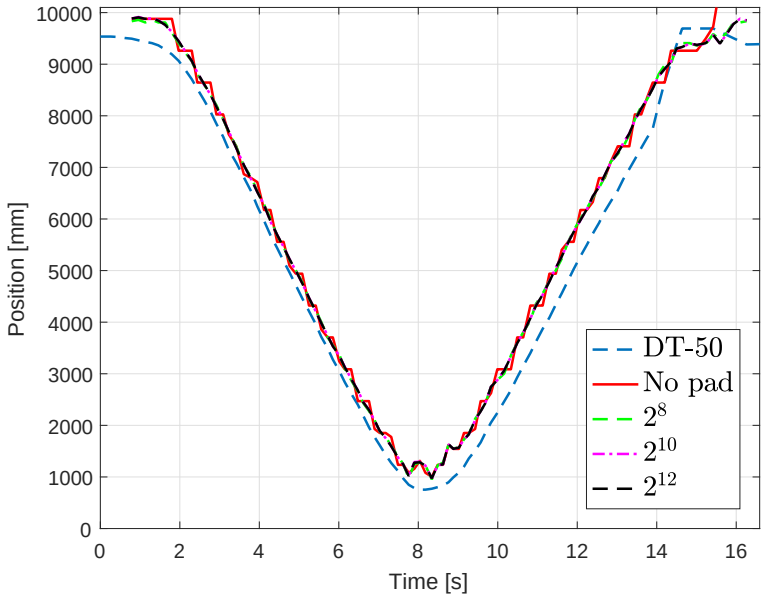

Figure 25: Range estimated from data acquired with a triangular chirp $2 \times T = 500$ µs in duration. Zero padded lengths specified in legend.

The total duration of the triangular chirp is increased to $2 \times T = 500$ µs. As in the previous section, reference data acquired with the DT50 is illustrated with the dashed blue line in Figure 25. The test procedure was essentially the same here as in the previous section, except that walking speed of the test subject might have varied slightly. Also, since time step due to UART delay was longer, the number of chirps collected could be decreased.

As previously, range estimated from the unpadded data can be seen to change in steps that approximately correspond to the calculated range resolution of 0.6 meters. Again, the steps are not exactly 0.6 meters for the same reason as before. Some samples have been dropped from the time series. Zero padding up to 2^8 can be seen to have a significantly smoothing effect. Longer paddings have a clearly diminished effect. Similarly to the previous results, zero paddings appears to cause the graphs to approach a final set of values. For example, when the subject is closest to the radar some jumps can be seen in the range estimation which have not smoothed out despite a very high zero padding.

A systematic error in estimated range can be seen here as well, and like previously, it is more pronounced when the target is moving away from the measurement setup. Zero padding appears to have no effect on this error, which would suggest that it is something inherent in the measurement.

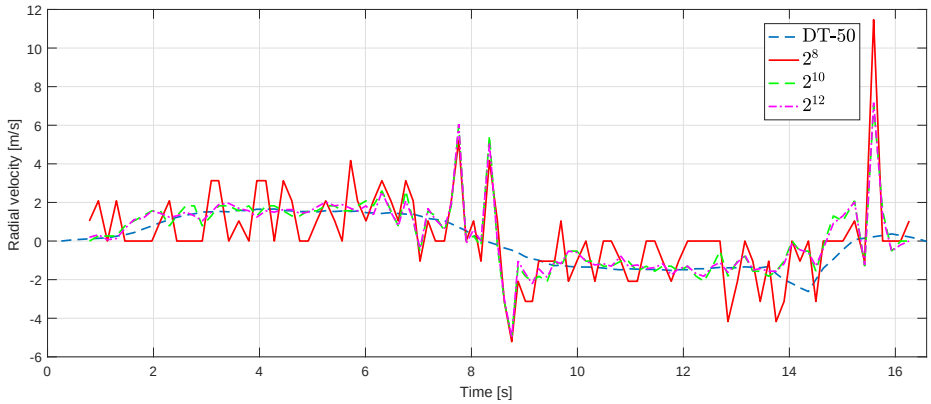

Figure 26: Radial velocity estimated from data acquired with a triangular chirp $2 \times T = 500$ µs in duration.

The effect of zero padding on estimated radial velocity is illustrated in Figure 26. As previously, the dashed blue line represents reference data acquired with the DT50 sensor.

The increased duration of the chirp has clearly had a positive effect on the results overall. The first zero padding appears to still be very noisy, but seems to change in steps that are much smaller than before. It appears to correctly indicate direction of the movement. However, the frequency resolution is still too coarse for an accurate estimation of instantaneous radial velocity.

Increasing the zero padding to 2^{10} appears to have an improved effect from the 250 µs chirp. The radial velocity overall appears to be very close to the reference data. As previously, the effect is diminished for each increase in padded length. The graphs seem to approach a set of final values that still have some inherent noise in them. However, the apparent final values are much closer to the reference data and overall provide a much more coherent picture. With sufficient padding, this chirp duration would appear to be reasonably accurate for estimating instantaneous radial velocity of the walking target.

As with the previous results, there are also high errors in the estimated radial velocity that are not smoothed by the zero padding. They can be observed especially at the start, halfway point, and end of the measurements.

5.3.1.2.3 1000 microseconds

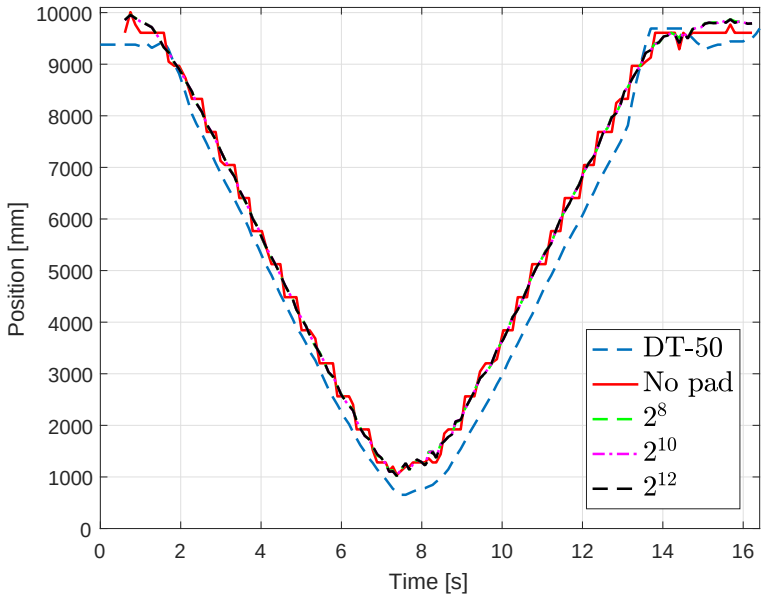

Figure 27: Range estimated from data acquired with a triangular chirp $2 \times T = 1000$ µs in duration. Zero padded lengths specified in legend.

The total duration of the triangular chirp is again doubled to 1000 µs. The estimate range is illustrated in Figure 27, with the reference data drawn in dashed blue line. Due to the increased UART delay, the number of chirps was decreased. Again, the test subject walked back and forth in front of the radar, possibly with some natural changes in walking speed.

Consistently with the previous results, the unpadded range estimation can be seen to change in steps that approximately correspond to 0.6 meters. However, the steps are more difficult to see as the plateaus between them are shorter in samples and thus duration. Zero padding can still be seen to have a smoothing effect, similarly to the previous results. Although the effect appears to be less pronounced, it should be kept in mind that this is due to the time step being much longer. If signal processing was done on the device, the steps in unpadded range estimation would be much clearer. Zero padding would also appear to be much more effective.

A systematic error can be seen to persist in these results as well. As previously, zero padding appears to have no effect on it.

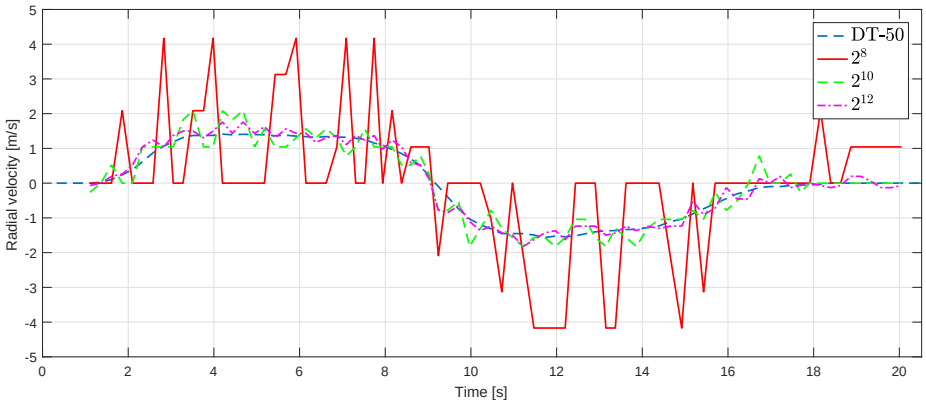

Figure 28: Radial velocity estimated from data acquired with a triangular chirp $2 \times T = 1000$ µs in duration.

The effect of zero padding on estimated radial velocity of the walking target is illustrated in Figure 28. Reference data acquired with the DT50 sensor is represented by the dashed blue line.

Overall it can be seen that zero padding appears to be even more effective as the duration of the triangular chirp increases. The effect and behavior of the first zero padding can be seen to be very similar to the previous results. The main difference is that for a longer chirp duration the set of final values that is approached with longer paddings appears to be more accurate. Graphs corresponding to 2^8 and 2^{10} paddings appear to follow the reference data much more accurately than in the previous results. Similarly, the smoothing effect of zero padding is also diminished for longer paddings. A padding of 2^{12} imroves the results further, but with a diminished effect.

It would seem that a moderate zero padding can be used to smooth out the actual radial velocity from the unpadded and very discontinuous data. As the chirp duration is increased, this final result is more reliably in line with the actual radial velocity of the target.

These results appear to be very valid for estimating the instantaneous radial velocity of the target, given a sufficient zero padding. It can also be seen that, same as before, there are some spikes in the estimation which are not smoothed away by the padding. They are much less severe, however.

5.3.1.2.4 Noise and effect of channel averaging

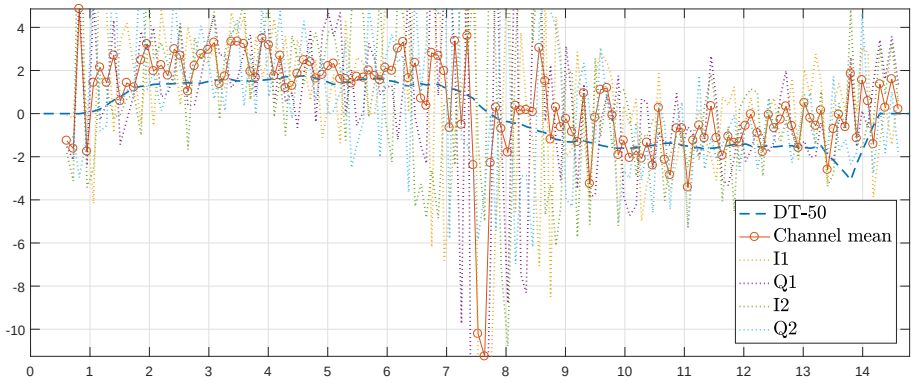

(a)

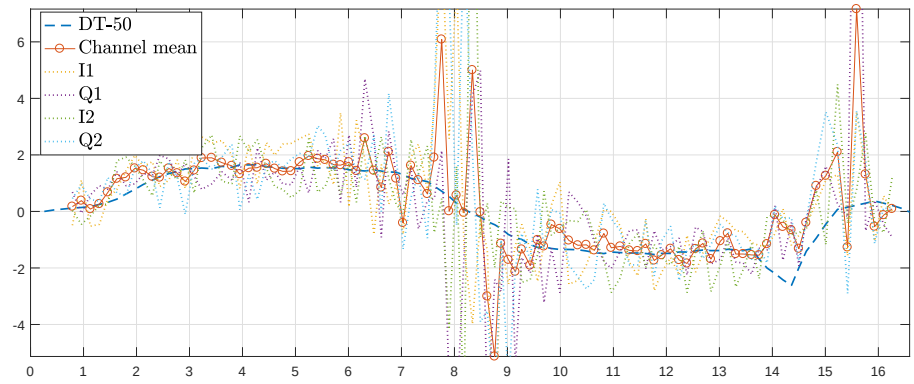

(b)

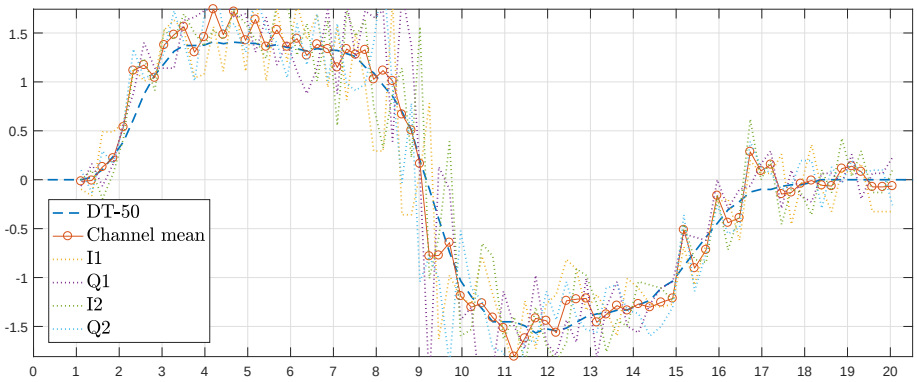

(c)

Figure 29: The noise cancelling effect of channel averaging with (a) $2 \times T = 250$ µs chirp, (b) $2 \times T = 500$ µs chirp, and (c) $2 \times T = 1000$ µs chirp.

The effect of channel averaging on estimated radial velocity is demonstrated in Figure 29. Resulting radial velocity of the walking target is plotted for each of the chirp

durations using a zero padding of 2^{15}. The dashed blue line represents the reference data, and the dotted lines each individual channel. Channel mean is illustrated with a solid red line and circular markers.

Earlier, the 250 µs chirp was concluded to be very noisy, and unaffected by increased zero padding. Figure 29a clearly shows how the individual channels are even noisier themselves. Channel averaging results in a reduced noise amplitude. It can also be seen that even though high errors in individual channels mostly cancel each other out, some large jumps persist. This can be seen between the 7 and 8 second marks.

Figure 29b shows that when the chirp duration is doubled to 500 µs, the individual channels are much less noisy by themselves. This also results in their mean being less noisy. Similarly to the 250 µs chirp, some strong errors persist despite zero padding and averaging. These can be seen especially around the 8 and 9 second marks, and at the end of the measurement.

Finally, Figure 29c demonstrates the 1000 µs chirp is the least noisy. Noise in the individual channels cancelled out by the averaging is also seen clearly. Especially when the walking target reverses direction, the averaging can be seen to give very accurate results. The error in individual channels is high at around the 9 second mark, but their average follows the reference closely. This is also the point where shorter chirps were seen to have high errors despite averaging. Similarly to the shorter chirps, some relatively strong errors that have not been corrected by the averaging can be observed at around the 17 second mark.

5.3.1.2.5 Deviation from reference

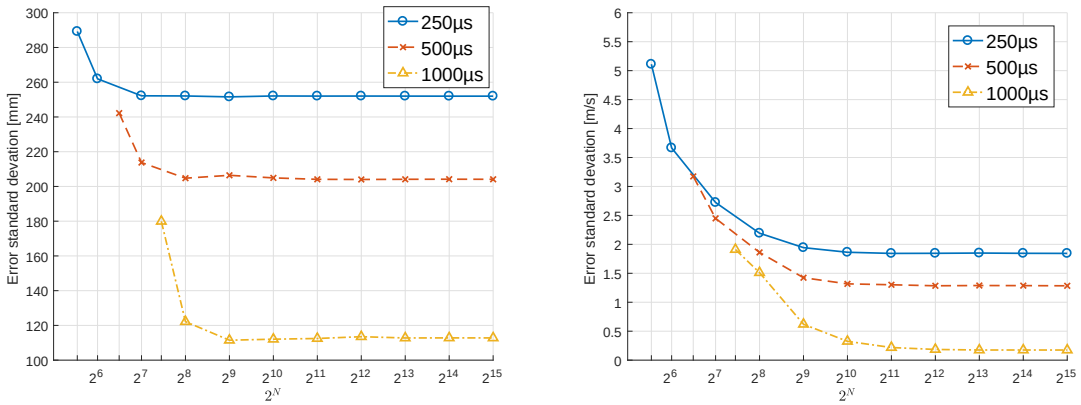

(a) (b)

Figure 30: Standard deviation of difference between the DT50 reference data and target parameters estimated with different triangular chirp durations in an anechoic chamber. (a) Position, and (b) radial velocity.

An error analysis is performed on the results acquired with different triangular chirp durations. This is performed by analysing how they differ from reference data acquired with the DT50 sensor. The difference between the estimated target parameters and reference data is calculated for each sweep using a range of zero paddings. Analysis is done with padded lengths ranging from unpadded data to 2^{15}. Standard deviations of the differences are illustrated in Figure 30. The first data points correspond to the results acquired with unpadded data.

The standard deviation of range estimation error is illustrated in Figure 30a. As was pointed out while analysing the range estimation graphs, the first zero padding greatly improves the results. Longer paddings have a diminished effect. This can also be observed in the figure. The standard deviation quickly plateaus after the second padding for each chirp duration. The plateaus are reached with zero paddings of 2^7, 2^8, and 2^9 with the durations in their respective orders.

It can also be observed that the plateau is lowered if the duration of the chirp is increased. This is an interesting observation, as the noise for each measurement should be practically the same. It seems that a longer chirp is less affected by the noise.

The standard deviation of radial velocity estimation is illustrated in Figure 30b. A very similar dependence on zero padded length can be observed here as well. Increased zero padding causes the standard deviation to decrease with a diminishing effect until a plateau is reached. However, this plateau requires a longer zero padding to reach when compared to standard deviation in range error. These lengths appear to be 2^9, 2^{10}, and 2^{11}, respectively.

Interference from the environment should, for all intents and purposes, be the same in each measurement. The noise appears to have a reduced effect on the results with an increased chirp duration. The accuracy of the results can be improved with zero padding to a certain extent, but a plateau is finally reached. It appears that magnitude of the plateau decreases with an increased chirp duration.

Earlier it was observed that graphs of the estimated target parameters appear to approach some final set of values as zero padding was increased. This can be seen in the standard deviation approaching a value as well. It seems that extracting the final values of radial velocity is more difficult, as it requires a longer zero padding to plateau. An interesting observation is also that the final value of the radial velocity standard deviation appears to be approximately inversely proportional to the chirp duration. Doubling the chirp duration approximately halves the standard deviation. The reason for this is discussed in more detain in Section 6.2

5.3.2 Stationary target

5.3.2.1 Measurement setup

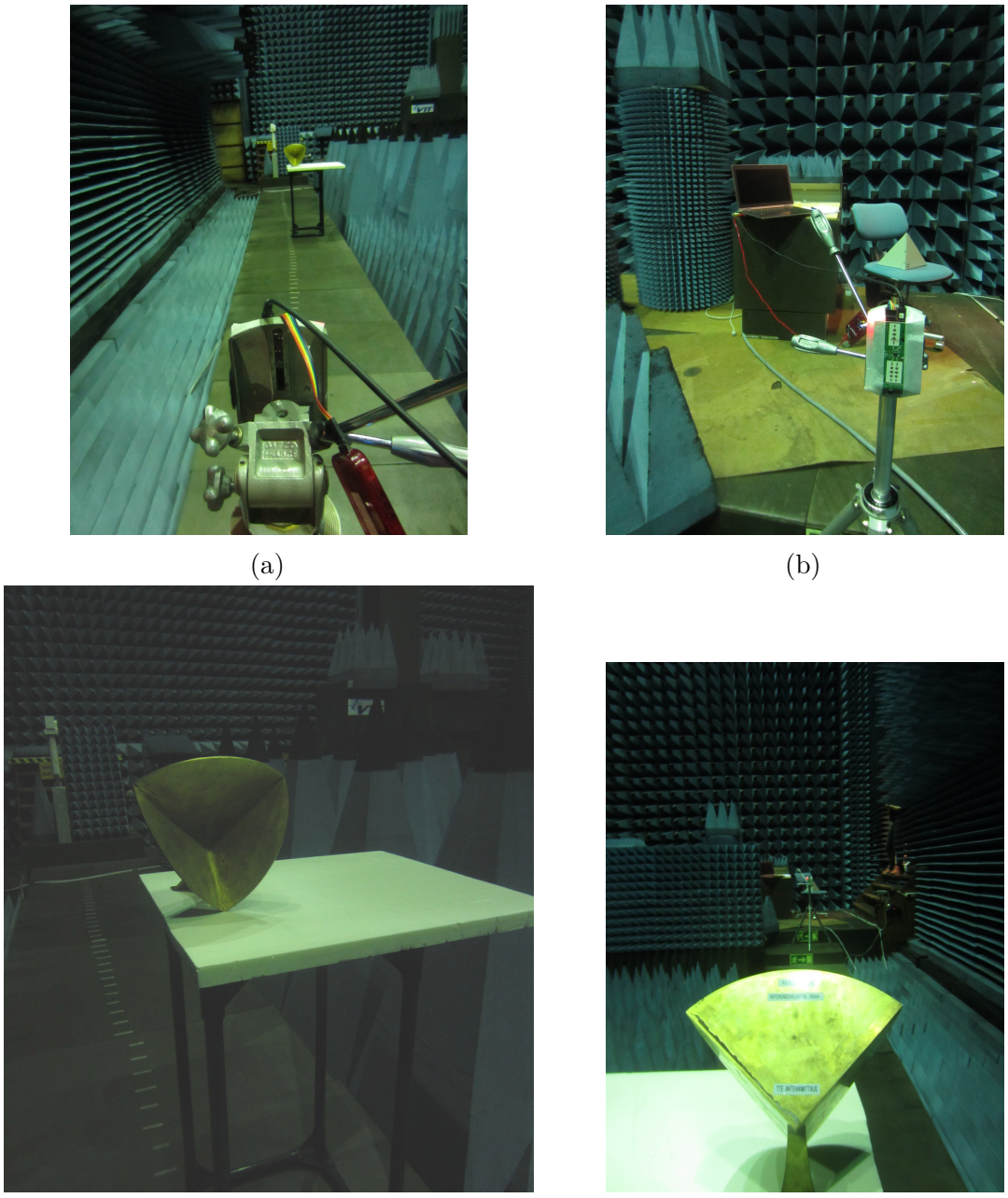

(a) (b) (c) (d)

Figure 31: Measurement setup in the anechoic chamber. (a) A view down the testing range. (b) A front view of the measurement setup. (c) A close-up of the corner reflector and table. (d) A view from behind the corner reflector.

To study how noise affects the estimated position and radial velocity of a target, an additional set of measurements were carried out. The setup of the measurement

is illustrated in Figure 31. Rather than a moving target, a stationary target was used instead. The target would remain in a fixed range and should exhibit a radial velocity of 0 meters per second. This should allow the noise susceptibility of a range of zero paddings and chirp durations to be assessed. A generic corner reflector was used as the stationary target. It was placed on a table consisting of plastic and foam at a distance of approximately 4.85 meters.

Other than generated chirp durations and corresponding lengths of sampled time series, no changes were made to the radar device. The sampling period remained as $T_s = 2.925$ µs. Total lengths of the time series ranged from 76 to 520, and were linearly dependent on chirp duration. Figure 31a presents a view down the range with the radar and stationary target visible. A frontal view of the setup is presented in Figure 31b, the DT50 sensor now being absent. A more detailed view of the stationary target is shown in Figure 31c and Figure 31d.

Measurements were performed with a range of chirp durations, ranging from a total triangular chirp duration of 200 µs to 1500 µs. The position and radial velocity of the target over time were estimated with a total of 100 chirps for each individual duration. The data was analyzed using a range of zero padded lengths, from no padding up to a padded length 2^{18}. The anechoic chamber was a very low noise environment, so a long zero padding was required to find the final set of values for each duration.

5.3.2.2 Results

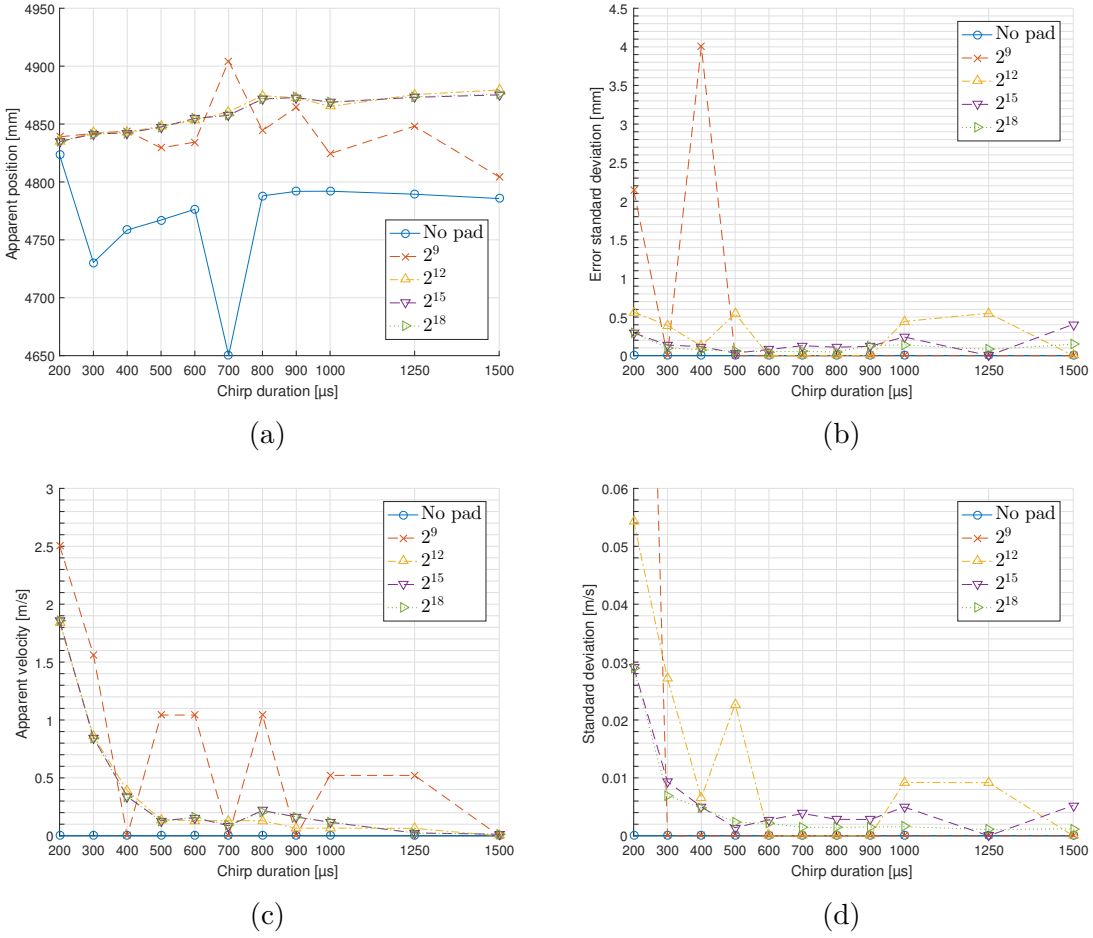

Figure 32: Measurement results of a stationary target. (a) Apparent position, and (b) standard deviation of position. (c) Apparent radial velocity, (d) standard deviation of radial velocity.

Measurement results with a stationary target are presented in Figure 32. The apparent position of the stationary target was estimated by calculating the position corresponding to each chirp, and taking a simple mean of the position. The resulting position as a function of chirp duration is illustrated in Figure 32a for a range of zero padded lengths. The standard deviation of position estimated with each chirp duration is illustrated in Figure 32b for a range of zero padded lengths.

Similarly, the apparent radial velocity of the stationary target is estimated by calculating it for each sweep and then calculating their mean. The apparent radial velocity as a function of chirp duration is illustrated in Figure 32c for a range of zero padded lengths. Finally, the noise susceptibility of the radial velocity estimation is analyzed by calculating its standard deviation for each chirp duration. This is illustrated in Figure 32d for a range zero padded lengths.

The distance to the target was measured to be approximately 4.85 meters. Figure 32a shows that the estimated position of the target seems to depend on both the length of zero padding and duration of the chirp. For a given chirp duration, increasing he zero padding seems to cause the estimated position to approach a final value. The effect of increased padding can be seen to diminish rapidly. Change from no padding to 2^9 can be seen to have a significant effect, whereas from 2^{12} to 2^{15} and 2^{18} almost no cange can be observed.

The estimated position of the target also seems to depend on the chirp duration, although not very significantly. The final values reached with a zero padding of 2^9 and longer are all within 50 millimeters of each other. As the length of zero padding and chirp duration increase, the estimated position can be seen to approach a value of approximately 4875 millimeters.

Overall, the estimated position appears to be very stable. Without padding, there is no deviation at all because the subtle changes in position are too small to be detected by the coarse FFT. However, as the padding is increased the deviations become apparent. For a zero padding of 2^{12} and above, the deviation is consistently less than 0.5 millimeters. Overall the 2^9 padding appears to be too coarse to detect anything other than some relatively large anomalies at 200 µs and 400 µs.

The estimated radial velocity of the stationary target appears to have some sort of permanent offset, which can be observed in Figure 32c. The offset is too small to be detected from the unpadded data, but becomes apparent after the first padding. This means that the ramp up and down section frequency peaks are somehow permanently shifted apart, rather than in the same position as they should be. It can also be seen that the offset decreases as chirp duration increases. Similarly to the previous results, the radial velocity seems to approach a final value for a given chirp duration as the zero padding is increased. There seems to be very little difference between the 2^{15} and 2^{18} paddings. For longer paddings, the effect of chirp duration on the offset becomes more clear. The offset is approximately inversely proportional to the chirp duration. Doubling the duration appears to halve the offset.

Even with the apparent offset, the estimated radial velocity of the stationary target appears to be very stable. Figure 32d shows that the standard deviation also decreases as the chirp duration increases. It appears to approach some final value as the padded length increases, similarly to the other parameters. However, since the noisiness of the estimation is so small inside the anechoic chamber, a very lengthy padding is required to bring this effect out.

5.4 Office setting

5.4.1 Measurement setup

(a)

(b)

Figure 33: Measurement setup indoors. (a) View down the test range from a distance of approximately 7 meters. (b) Back view of the measurement setup and test range. Note the two pillars.

Due to the success of the previous measurements, the tests involving a walking target are repeated indoors in an office environment. A long corridor inside a VTT office building acted as the testing range. Since the measurements were performed without help this time, the author acted as the test subject. The test subject started from approximate one meter away from the measurement setup, walked briskly to a distance of approximately seven meters, and then walked back. The test range is illustrated in Figure 33. Except for the location, the parameters of the equipment remain identical to the previous section.

The corridor had multiple open doors to offices and workshops on both of its sides. At distances of approximately one meter and seven meters there were two large columns on the right hand side of the corridor. The location was chosen due to its length to allow for a measurement of similar duration to the previous one. A closed office space was also useful in assessing how the target parameter estimation was affected by outside interference, such as reflections from multiple targets.

The measurements were performed for a range of chirp durations, but only results for the 1000 µs chirp are presented. This is because they were concluded to be most representative of the triangular chirp's accuracy and robustness. Zero paddings of 2^8, 2^{10}, and 2^{12} will be considered.

5.4.2 Results

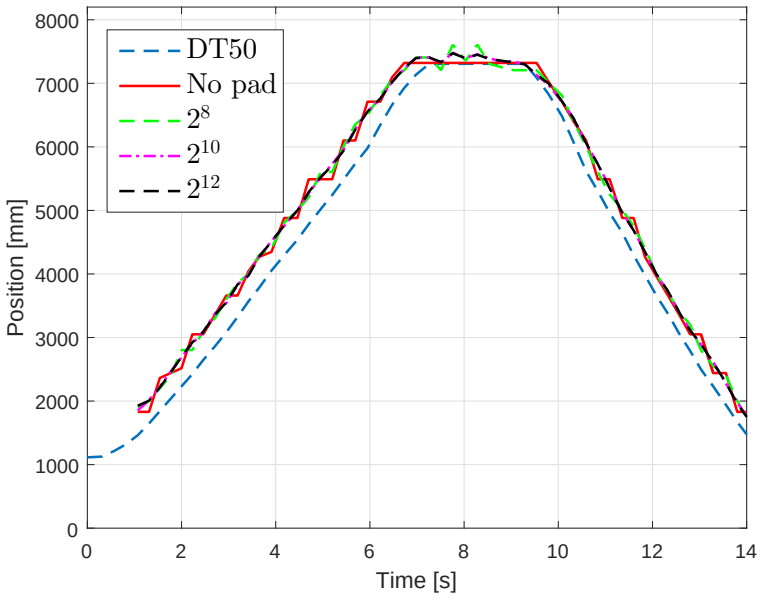

Figure 34: Range estimated from data acquired with a triangular chirp $2 \times T = 1000$ µs in duration. Zero padded lengths specified in legend.

The total duration of the triangular chirp was 1000 µs. The resulting range estimations for different zero padded lengths are illustrated in Figure 34.

Similarly to the results acquired in an anechoic chamber, the steps in unpadded range estimation have become harder to see. This is again due to the number of chirps being decreased since the UART delay is longer. Higher zero paddings seem to yield little improvement in range estimation.

A systematic error similar to all the previous range estimations persists in these results as well.

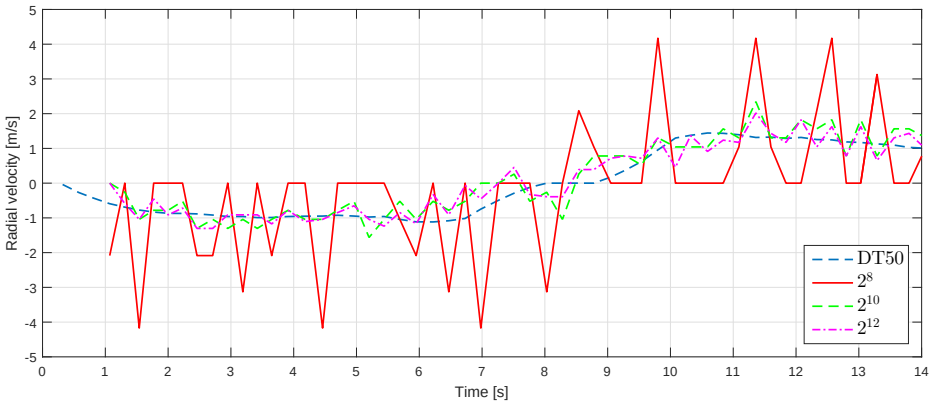

Figure 35: Radial velocity estimated from data acquired with a triangular chirp $2 \times T = 1000$ µs in duration. Zero padded lengths specified in legend.

The effect of zero padding on estimated radial velocity of the target is illustrated in Figure 35. Reference data acquired with the DT50 is illustrated with the dashed blue line.

Zero padding can be seen to affect the results very similarly to the anechoic chamber section. The first zero padding is still too coarse to estimate the instantaneous radial velocity of the target. Still, it seems to accurately indicate the presence and direction of a moving target. Each successive increase in zero padded length causes the graph to approach the final set of values. The graphs obtained with 2^{10} and 2^{12} zero paddings are very close to the reference data. It is clear that the instantaneous radial velocity of a moving target can be estimated very accurately even in an environment with multiple sources of interference.

5.5 Summary of results and observations

5.5.1 Procedure and setup of measurements

In this section, a large number of results were presented. Measurements were performed with a range of triangular chirp durations, and their effectiveness in estimating the position and radial velocity of a single target were assessed. Only the duration of the transmitted chirp was considered, as altering other parameters of the radar device was not feasible.

Measurements were performed in two distinct environments. Procedure and setup of the measurements were the same in both of them. A person holding a corner reflector was used as a test subject. The position and apparent velocity of a stationary target were also considered. First, a large anechoic chamber was used as a testing ground. This was done to demonstrate phenomena relevant to target detection with a triangular chirp as clearly as possible. The chamber eliminated possible sources of

outside interference.

The same measurements were repeated in an office environment. This was done to demonstrate robustness of the method in a more realistic scenario.

5.5.2 Effect of zero padding and chirp duration

Measurements were performed in the anechoic chamber using a range of chirp durations, and the data was processed using different zero padded lengths. The measurements can be considered to have been successful. It was demonstrated that zero padding the raw data can greatly improve accuracy in estimating the position and radial velocity of a target.

The presented results demonstrate that estimated target parameters are susceptible to outside interference in a manner that is approximately inversely proportional to duration of the chirp. Increased chirp duration yields more accurate results. Raw data can be zero padded before signal processing to increase accuracy further, but only up to a certain point. With longer zero paddings, the graph of estimated radial velocity seemed to approach some final set of values. The longer the chirp was, the more accurately this final graph followed reference data.

The results suggest that accurately estimating the position of a target is easier than its radial velocity. Even with a relatively short chirp of 250 µs, raw unpadded data yields reasonably accurate results. However, even using a relatively long chirp of 1000 µs it is not feasible to estimate instantaneous radial velocity of a moving target from raw data. It was shown that the presence and direction of a moving target can be indicated correctly, but the resolution is too coarse. Without greatly increasing chirp duration, zero padding is required to estimate radial velocity.

5.6 Quality of results

Radial velocity estimated with 250 and 500 µs was found to be too noisy for targets moving at walking speeds. With a sufficiently long zero padding, they had standard deviations of 2.5 and 1.25 m/s, respectively. These results followed general trend of the reference data well, but were not sufficiently accurate for reliably estimating the instantaneous radial velocity of the target.

Results obtained with a 1000 µs chirp were found to be extremely accurate. The graph of the estimated radial velocity coincided with the reference data very well. Noisiness of the results were also low enough to clearly see that radial velocity for practically all measurement points was very accurate. The standard deviation of difference to the reference data was approximately 0.25 meters per second. In practice, this means that 68.2% of data points were within 0.25 m/s of the highly accurate

reference data.

This was a clear improvement over the shorter durations, where the instantaneous radial velocities had comparatively high errors. The 1000 µs chirp was shown to be sufficiently accurate to estimate the target's radial velocity at any given moment in time.

Due to success of measurements in the anechoic chamber, they were repeated in a more realistic environment. The 1000 µs chirp was shown to maintain its accuracy, proving its robustness and potential for practical applications.

6 Conclusion

This section presents a summary of conclusions that can be made from presented experimental results.

6.1 Measurement setup

Measurement setups and procedures described in Section 5 were found to be simple and effective. Reproducing presented experiments should not be challenging. All procedures can be carried out by a single person.

Only point of contention in these results might be length of the time step between each measured data point. Due to UART link data transfer delay, it was very long in comparison to chirp duration. A shorter time step could be realized, but this would require an alternative data transfer protocol, or changing programming of the microcontroller. Regardless, the results are very illustrative. If the presented method is implemented on the microcontroller itself, time between successive measurements will naturally be much shorter.

6.2 Measurement results

Results obtained in both the anechoic chamber and office environment were excellent. The graphs presented in Section 5.3 demonstrate that the zero padding of a triangular chirp can significantly increase the accuracy of radial velocity estimation. A relatively short triangular chirp can be used while maintaining high accuracy. Much higher radial velocities are detectable than with slow-time processing. Both are clear improvements over slow-time processing. A disadvantage is the need for frequency pairing in a multi target situation, although this could be offset by the much shorter total chirp duration.

It was shown that the error in estimated range and the radial velocity of a target was approximately inversely proportional to the duration of the triangular chirp. This was shown to be the case with both a moving and stationary targets. A longer chirp naturally means more actual data samples in addition to zero padded samples.

It was discovered that zero padding had a diminishing effect up to a certain point, depending on chirp duration. This would suggest that there was some accuracy limit in the measurements.

Inverse proportionality to chirp duration can be explained by the Cramer-Rao lower bound (CRLB) [87], which defines the accuracy limits of estimating a sine wave from a set of noisy discrete samples. The limit depends on signal-to-noise ratio (SNR) of the device, and the number of samples. The more noise there is, the more difficult it is to accurately reconstruct the sine wave. In turn, a higher number of samples can increase the accuracy. The noise affects the apparent frequency of the sine wave, which is how it relates to FMCW radars.

A more concise explanation is provided in [76]. The publication demonstrates that the CRLB causes a statistical variance in range estimation with an FMCW radar in a noisy environment. The variance is inversely proportional to the number of samples used. The variance of the estimated range should therefore decrease when the number of samples is increased. The accuracy of a zero padded FFT, along with other algorithms, is demonstrated to be limited by the CRLB.

Since radial velocity is estimated from the same FFT spectrum as range, it is reasonable to expect that it would behave in a similar manner. SNR of the radar device should practically be the same across all measurements in the same environment. Therefore, a longer chirp duration and a correspondingly increased number of samples should result in a lower error where the accuracy will reach a plateau.

This demonstrates that zero padding can be used to improve the accuracy only to a certain point. After the effect begins to diminish, the accuracy can be improved only with a longer chirp, or a shorter sampling interval.

Due to the success of measurements performed in the anechoic chamber, they were repeated in an office environment. The results were shown to more or less retain their accuracy. This demonstrates the method to be robust and ready for practical applications.

6.3 Distinction between resolution and accuracy

In Section 3.4 it was demonstrated that the position of a frequency peak in an FFT spectrum can be pinpointed more accurately using zero padding. This was demonstrated to be especially useful when comparing separate spectra from two different time series. However, this was found not to have an effect on distinguishing between two frequency peaks in the same FFT spectrum.

The two separate spectra are analogous to up and down ramp sections of a triangular chirp. Finding the values of the peaks more accurately allows far more accurate estimation of the Doppler shift and radial velocity. Zero padding has a

similar effect on the range estimation as well. Note that this only improves the accuracy of the estimation, not actual resolution of the radar.

Some earlier publications refer to an improved resolution when describing the effects of zero padding and some other means of interpolation [55, 56, 76]. What is actually being improved is ability to pinpoint the range of a specific target, not distinguishing two targets. The range resolution of an FMCW radar is the minimum distance between two targets where they still appear as separate [1, 7, 15]. This can only be improved with a broader sweep bandwidth.

It was demonstrated that zero padding increases the accuracy of the FFT, not the resolution. Distinction between the resolution and accuracy of FMCW measurements is correctly highlighted in [57]. Similarly, the results of interpolation are correctly referred to as improved accuracy in [78]. Although some [54] methods are capable of detecting targets that are too close to be resolved with FFT, it is still reasonable to maintain a clear distinction between the accuracy and resolution of FMCW measurements.

6.4 Future research

Only single target measurements were considered in these measurements. In many practical applications this is an unlikely scenario. Pairing algorithms for waveforms that produce multiple beat frequencies for one target have been a subject of intense study [62, 66, 67, 68]. For the presented method to be truly practically viable, it needs to be able to effectively recognize real targets and avoid detection of ghost targets.

An offset was observed when estimating the radial velocity of a stationary target in Section 5.3.2. The offset seemed to be inversely proportional to the chirp duration, and decreased quickly as the duration increased. Despite this, an investigation into why short chirp durations displayed such a high offset could be in order.

All signal processing was done outside the radar device itself. Data was transferred to a laptop, which handled the long and demanding FFTs. For practical purposes, signal processing should be realized on the microcontroller of the radar device. This would introduce limited resources in terms of time and computing power to the data. Only the effect of zero padding on accuracy was considered, not how time-efficient it actually was.

It has been demonstrated that the radial velocity and position of a target can be estimated with a high accuracy by means of increasing accuracy of FFT. Other methods of enhancing beat frequency accuracy should be considered, such as chirp z-transform [52, 53], ESPRIT algorithm [54], and frequency estimation [88, 89]. They should be contrasted with the simple zero padding in terms of their computational requirements to produce more practical solutions.

References

[1] M. I. Skolnik, *Introduction to Radar Systems*. New York, NY: McGraw-Hill, 2001.

[2] R. Colton, "Radar in the United States Army History and Early Development at the Signal Corps Laboratories, Fort Monmouth, N.J." *Proceedings of the IRE*, vol. 33, no. 11, pp. 740–753, 1945.

[3] W. C. Tinus and W. H. C. Higgins, "Early fire-control radars for Naval Vessels," *The Bell Systems Technical Journal*, vol. 25, no. 1, pp. 1–47, 1946.

[4] A. A. Kostenko, A. I. Nosich, and I. A. Tishchenko, "Development of the first Soviet three-coordinate L-band pulsed radar in Kharkov before WWII," *IEEE Antennas and Propagation Magazine*, vol. 43, no. 3, pp. 29–48, 2001.

[5] G. Sato, "A Secret Story About the Yagi Antenna," *IEEE Antennas and Propagation Magazine*, vol. 33, no. 3, pp. 7–18, 1991.

[6] K. Barton, "A Half Century of Radar," *IEEE Transactions on Microwave Theory and Techniques*, vol. 32, no. 9, pp. 1161–1170, 1984.

[7] B. A. Atayants, V. M. Davydochkin, V. V. Ezerskiy, V. S. Parshin, and S. M. Smolskiy, *Precision FMCW Short-Range Radar for Industrial Applications*. Norwood, MA: Artech House, 2014.

[8] J. O. Bentley, "Airplane altitude indicating system," U. S. Patent No. 2,011,392, issued August 13, 1935, application August 10, 1928.

[9] Y. Fan, Z. Yang, X. Bu, and J. An, "Radar waveform design and multi-target detection in vehicular applications," in *2015 International Conference on Estimation, Detection and Information Fusion (ICEDIF)*, Jan 2015, pp. 286–289.

[10] H. J. Ng, A. Fischer, R. Feger, R. Stuhlberger, L. Maurer, and A. Stelzer, "A DLL-supported, low phase noise fractional-N PLL with a wideband VCO and a highly linear frequency ramp generator for FMCW radars," *IEEE Transactions on Circuits and Systems I: Regular Papers*, vol. 60, no. 12, pp. 3289–3302, 2013.

[11] P. Molchanov, S. Gupta, K. Kim, and K. Pulli, "Short-range FMCW monopulse radar for hand-gesture sensing," in *2015 IEEE Radar Conference (RadarCon)*, May 2015, pp. 1491–1496.

[12] H. Rohling and C. Moller, "Radar waveform for automotive radar systems and applications," *2008 IEEE Radar Conference*, vol. 1, no. 1, pp. 1–4, 2008.

[13] S. Jardak, T. Kiuru, M. Metso, P. Pursula, J. Häkli, M. Hirvonen, S. Ahmed, and M. S. Alouini, "Detection and localization of multiple short range targets using fmcw radar signal," in *2016 Global Symposium on Millimeter Waves (GSMM) ESA Workshop on Millimetre-Wave Technology and Applications*, June 2016, pp. 1–4.

[14] M. A. Richards, *Funtamentals of Radar Signal Processing.* New York, NY: McGraw-Hill, 2005.

[15] I. Komarov and S. Smolskiy, *Fundamentals of Short-Range FM Radar.* Norwood, MA: Artech House, 2003.

[16] J. Ryde and N. Hillier, "Performance of Laser and Radar Ranging Devices in Adverse Environmental Conditions," *Journal of Field Robotics*, vol. 26, no. 9, pp. 712–727, Sept 2009.

[17] K. M. Strohm, H. L. Bloecher, R. Schneider, and J. Wenger, "Development of future short range radar technology," in *European Radar Conference (EURAD)*, Oct 2005, pp. 165–168.

[18] S. Worrall, "Providing situation awareness in complex multi-vehicle operations," Ph.D. dissertation, University of Sydney, Sydney, Australia, March 2009.

[19] B. Clarke, S. Worrall, G. Brooker, J. Martinez, and E. Nebot, "Improving situational awareness with radar information," in *Intelligent Vehicles Symposium (IV), 2012 IEEE*, June 2012, pp. 535–540.

[20] H. L. Bloecher, J. Dickmann, and M. Andres, "Automotive active safety & comfort functions using radar," in *2009 IEEE International Conference on Ultra-Wideband*, Sept 2009, pp. 490–494.

[21] Y. Han, Z. Shao, Y. Yang, X. Zhu, and L. Liu, "The research of homodyne LFMCW radar," *2012 International Conference on Computational Problem-Solving, ICCP 2012*, pp. 281–283, 2012.

[22] T. Fujibayashil, Y. Takeda, W. Wangl, V.-s. Yeh, W. Stapelbroek, S. Takeuchi, and B. Floyd, "A 76- to 81-GHz Packaged Single-Chip Transceiver for Automotive Radar," in *2016 IEEE Bipolar/BiCMOS Circuits and Technology Meeting (BCTM)*, 2016, pp. 166–169.

[23] J. Wursthorn, H. Knapp, J. Al-Eryani, K. Aufinger, S. Majied, S. Boguth, H. Li, R. Lachner, and L. Maurer, "SiGe power amplifier for automotive radar applications from 76 to 81 GHz," *2016 IEEE MTT-S International Conference on Microwaves for Intelligent Mobility, ICMIM 2016*, pp. 3–6, 2016.

[24] R. K. Mishra, D. K. Srivastav, K. Srinivasan, V. Nandi, and R. R. Bhat, "Impact of Foreign Object Damage on an Aero Gas Turbine Engine," *Journal of Failure Analysis and Prevention*, vol. 15, no. 1, pp. 25–32, 2015.

[25] P. D. L. Beasley, G. Binns, R. D. Hodges, and R. J. Badley, "Tarsier, a millimetre wave radar for airport runway debris detection," in *First European Radar Conference*, Oct 2004, pp. 261–264.

[26] H. Essen, F. Lorenz, S. Hantscher, P. Warok, R. Zimmermann, M. Schröder, W. Koch, M. Schikora, G. Luedtke, and K. Wild, "Millimeterwave [sic] radar for runway debris detection," in *2011 Tyrrhenian International Workshop on Digital Communications - Enhanced Surveillance of Aircraft and Vehicles (TIWDC/ESAV)*, Sept 2011, pp. 65–68.

[27] P. Feil, W. Menzel, T. P. Nguyen, C. Pichot, and C. Migliaccio, "Foreign Objects Debris Detection (FOD) on Airport Runways Using a Broadband 78 GHz Sensor," in *38th European Microwave Conference*, Oct 2008, pp. 1608–1611.

[28] M. Rangwala, F. Wang, and K. Sarabandi, "Study of Millimeter-Wave Radar for Helicopter Assisted-Landing System," *IEEE Antennas and Propagation Magazine*, vol. 50, no. 2, pp. 13–25, April 2008.

[29] M. Rangwala, J. Lee, and K. Sarabandi, "Design of FMCW millimeter-wave radar for helicopter assisted landing," in *2007 IEEE International Geoscience and Remote Sensing Symposium*, July 2007, pp. 4183–4186.

[30] C. Migliaccio, B. D. Nguyen, C. Pichot, N. Yonemoto, K. Yamamoto, K. Yamada, H. Nasui, W. Mayer, A. Gronau, and W. Menzel, "Millimeter-wave radar for rescue helicopters," in *2006 9th International Conference on Control, Automation, Robotics and Vision*, Dec 2006, pp. 1–6.

[31] J. Y. Lee, K. B. Lee, and S. H. Choi, "A Design of Motion Detecting Sensor using Microwave," in *2007 Asia-Pacific Microwave Conference*, Dec 2007, pp. 1–4.

[32] T. Kiuru, M. Metso, S. Jardak, P. Pursula, J. Häkli, M. Hirvonen, and R. Sepponen, "Movement and respiration detection using statistical properties of the FMCW radar signal," in *2016 Global Symposium on Millimeter Waves (GSMM) ESA Workshop on Millimetre-Wave Technology and Applications*, June 2016, pp. 1–4.

[33] P. Bernardi, R. Cicchetti, S. Pisa, E. Pittella, E. Piuzzi, and O. Testa, "Design, Realization, and Test of a UWB Radar Sensor for Breath Activity Monitoring," *IEEE Sensors Journal*, vol. 14, no. 2, pp. 584–596, Feb 2014.

[34] D. Dakopoulos and N. G. Bourbakis, "Wearable Obstacle Avoidance Electronic Travel Aids for Blind: A Survey," *IEEE Transactions on Systems, Man, and Cybernetics, Part C (Applications and Reviews)*, vol. 40, no. 1, pp. 25–35, Jan 2010.

[35] L. Scalise, V. M. Primiani, P. Russo, D. Shahu, V. D. Mattia, A. D. Leo, and G. Cerri, "Experimental investigation of electromagnetic obstacle detection for visually impaired users: A comparison with ultrasonic sensing," *IEEE Transactions on Instrumentation and Measurement*, vol. 61, no. 11, pp. 3047–3057, Nov 2012.

[36] S. Pisa, E. Piuzzi, and G. Affronti, "A FMCW Radar as Electronic Travel Aid for Visually Impaired Subjects," in *Measurement in Reseach and Industry*. Prague, Czech Republic: XXI IMEKO World Congress, 2015.

[37] S. Pisa, E. Pittella, and E. Piuzzi, "Serial Patch Array Antenna for an FMCW Radar Housed in a White Cane," *International Journal of Antennas and Propagation*, vol. 2016, pp. 1–10, 2016.

[38] S. Kim, I. Paek, and M. Ka, "Simulation and test results of triangular fast ramp FMCW waveform," in *2013 IEEE Radar Conference (RadarCon13)*, April 2013, pp. 1–4.

[39] M. Kashif, M. Yasin, N. Ahsan, and Z. Y. Malik, "Design, development and linearity testing of synthesized FMCW RF source," in *Proceedings of 2013 10th International Bhurban Conference on Applied Sciences and Technology, IBCAST 2013*, 2013, pp. 435–438.

[40] "All about direct digital synthesis," http://www.analog.com/en/analog-dialogue/articles/all-about-direct-digital-synthesis.html, accessed: 2016-12-14.

[41] V. Teppati, A. Ferrero, and M. Sayed, *Modern RF and Microwave Measurement Techniques*. Cambridge, UK: Cambridge, 2013.

[42] T. Musch, I. Rolfes, and B. Schiek, "A highly linear frequency ramp generator based on a fractional divider phase-locked-loop," *IEEE Transactions on Instrumentation and Measurement*, vol. 48, no. 2, pp. 634–637, April 1999.

[43] Y. T. Im, J. H. Lee, and S. O. Park, "A DDS and PLL-based X-band FMCW radar system," *2011 IEEE MTT-S International Microwave Workshop Series on Intelligent Radio for Future Personal Terminals, IMWS-IRFPT 2011*, pp. 4–5, 2011.

[44] H. Jianqiang, S. Kaiyun, and L. Zhenya, "Research on the Method for Producing a Highly Linear FMCW Signal Based on the PLL Circuits," in *3rd Asia-Pacific Conference on Antennas and Propagation Research*. Harbin, China: IEEE, 2014, pp. 1416–1419.

[45] B. J. Lipa and D. E. Barrick, *FMCW Signal Processing*. Sunnyvale, California: Mirage Systems, 1990.

[46] S. O. Piper, "Homodyne FMCW radar range resolution effects with sinusoidal nonlinearities in the frequency sweep," in *Proceedings International Radar Conference*, May 1995, pp. 563–567.

[47] M. Pichler, A. Stelzer, P. Gulden, and M. Vossiek, "Influence of systematic frequency-sweep non-linearity on object distance estimation in FMCW/FSCW radar systems," *Conference Proceedings - 33rd European Microwave Conference, EuMC 2003*, vol. 3, no. 5, pp. 1203–1206, 2003.

[48] S. Scheiblhofer, S. Schuster, and A. Stelzer, "Effects of systematic FMCW radar sweep nonlinearity on bias and variance of target range estimation," *IEEE MTT-S International Microwave Symposium Digest*, no. 5, pp. 1418–1421, 2006.

[49] H. A. Ahmed, A. N. Hafez, and A. H. Khalil, "Novel technique for reducing effects of non-linear frequency sweeps in LFM ranging radars," in *2009 4th International Design and Test Workshop (IDT)*, Nov 2009, pp. 1–5.

[50] M. Vossiek, P. Heide, M. Nalezinski, and V. Mágori, "Novel FMCW radar system concept with adaptive compensation of phase errors," in *1996 26th European Microwave Conference, EuMC 1996*, 1996, pp. 135–139.

[51] H. Rohling and C. Moller, "Radar waveform for automotive radar systems and applications," in *2008 IEEE Radar Conference*, May 2008, pp. 1–4.

[52] D. Li, H. Lin, H. Liu, H. Wu, and X. Tan, "Focus improvement for squint FMCW-SAR data using modified inverse Chirp-Z transform based on spatial-variant linear range cell migration correction and series inversion," *IEEE Sensors Journal*, vol. 16, no. 8, pp. 2564–2574, 2016.

[53] P.-C. Gong, J. Li, W. Guo, and Z. Shao, "A high resolution algorithm based on Chirp Z-transform for FMCW radar," in *2015 IEEE International Conference on Communication Problem-Solving (ICCP)*, Oct 2015, pp. 482–484.

[54] R. Roy, A. Paulraj, and T. Kailath, "Estimation of Signal Parameters via Rotational Invariance Techniques - ESPRIT," in *Military Communications Conference - Communications-Computers: Teamed for the 90's*, vol. 3, Oct 1986, pp. 41.6.1–41.6.5.

[55] Q. G. Q. Guoqing, "High accuracy range estimation of FMCW level radar based on the phase of the zero-padded FFT," in *2004 7th International Conference on Signal Processing, 2004. Proceedings*, vol. 3, 2004, pp. 2078–2081.

[56] Q. Guoqing and J. Xinle, "Improvement of measurement accuracy of FMCW level radar," in *2001 CIE International Conference on Radar Proceedings (Cat No.01TH8559)*, 2001, pp. 567–570.

[57] S. Ayhan, M. Pauli, T. Kayser, S. Scherr, and T. Zwick, "FMCW radar system with additional phase evaluation for high accuracy range detection," in *2011 8th European Radar Conference*, Manchester, UK, 2011, pp. 117–120.

[58] Y. Fan, K. Xiang, J. An, and X. Bu, "A new method of multi-target detection for FMCW automotive radar," in *IET International Radar Conference 2013*, April 2013, pp. 1–4.

[59] T. Y. Lee, S. Y. Jeon, J. Han, V. Skvortsov, K. Nikitin, and M. H. Ka, "A simplified technique for distance and velocity measurements of multiple moving objects using a linear frequency modulated signal," *IEEE Sensors Journal*, vol. 16, no. 15, pp. 5912–5920, Aug 2016.

[60] H. Rohling and M. M. Meinecke, "Waveform design principles for automotive radar systems," in *Radar, 2001 CIE International Conference on, Proceedings*, 2001, pp. 1–4.

[61] J.-J. Lin, Y.-P. Li, W.-C. Hsu, and T.-S. Lee, "Design of an FMCW radar baseband signal processing system for automotive application," *SpringerPlus*. [Online]. Available: http://dx.doi.org/10.1186/s40064-015-1583-5

[62] Q. Y. Liu, Y. X. Sun, Q. Zhang, and X. J. Liang, "Multi-target parameter estimation based on velocity compensation in FMCW radar," in *IET International Radar Conference 2015*, Oct 2015, pp. 1–4.

[63] E. Hyun and J. H. Lee, "A meothod [sic] for multi-target range and velocity detection in automotive fmcw radar," in *2009 12th International IEEE Conference on Intelligent Transportation Systems*, Oct 2009, pp. 1–5.

[64] H. Zhou, P. Cao, and S. Chen, "A novel waveform design for multi-target detection in automotive FMCW radar," in *2016 IEEE Radar Conference (RadarConf)*, May 2016, pp. 1–5.

[65] V. Winkler, "Range Doppler detection for automotive FMCW radars," in *2007 European Radar Conference*, Oct 2007, pp. 166–169.

[66] Y. Fan, K. Xiang, J. An, and X. Bu, "A new method of multi-target detection for FMCW automotive radar," in *IET International Radar Conference 2013*, April 2013, pp. 1–4.

[67] E. Hyun, W. Oh, and J. H. Lee, "Multi-target detection algorithm for FMCW radar," in *2012 IEEE Radar Conference*, May 2012, pp. 0338–0341.

[68] C. Yang, H. Tang, H. Jiang, and H. An, "Beat-frequency matching for multi-target based on improved trapezoid wave with FMCW Radar," in *2011 IEEE International Conference on Signal Processing, Communications and Computing (ICSPCC)*, Sept 2011, pp. 1–4.

[69] H. Rohling and M. M. Meinecke, "Waveform design principles for automotive radar systems," in *2001 CIE International Conference on Radar Proceedings (Cat No.01TH8559)*, 2001, pp. 1–4.

[70] B. Xin and D. Jinsong, "A new waveform for range-velocity decoupling in automotive radar," in *2010 2nd International Conference on Signal Processing Systems*, vol. 1, July 2010, pp. V1–511–V1–514.

[71] A. Hossen and U. Heute, "Two-dimensional subband transforms: theory and applications," *IEE Proceedings - Vision, Image and Signal Processing*, vol. 151, no. 5, pp. 389–399, Oct 2004.

[72] A. Gromek, R. Rytel-Andrianik, P. Samczynski, and L. Corucci, "Detection and tracking experiments with a fixed fmcw radar in an urban scenario," in *2014 15th International Radar Symposium (IRS)*, June 2014, pp. 1–5.

[73] M. Taghouti, D. Lucani, M. Pedersen, and A. Bouallegue, "On the impact of zero-padding in network coding efficiency with internet traffic and video traces," in *European Wireless Conference 2016, EW 2016*, 2016, pp. 72–77.

[74] Y.-J. Zhu, H. Xu, and Y.-Y. Zhang, "Zero-padding block transmission for underwater optical wireless communications," *Electronics Letters*, vol. 52, no. 4, pp. 298–300, 2016.

[75] S. Järvenpää and P. Ylä-Oijala, "Multilevel fast multipole algorithm with global and local interpolators," *IEEE Transactions on Antennas and Propagation*, vol. 62, no. 9, pp. 4716–4725, 2014.

[76] S. Scherr, S. Ayhan, M. Pauli, and T. Zwick, "Accuracy limits of a K-band FMCW radar with phase evaluation," in *2012 9th European Radar Conference*, Oct 2012, pp. 246–249.

[77] Z. Chengge and Y. Yeshu, "A method for target estimation of level radar," in *Proceedings of International Radar Conference*, 1996, pp. 270–273.

[78] M. Song, J. Lim, D. J. Shin, and J. Sohn, "Enhancing doppler estimation via newton interpolation for automotive fmcw radars," in *2014 International Conference on Information and Communication Technology Convergence (ICTC)*, Oct 2014, pp. 615–616.

[79] M. Frigo and S. G. Johnson, "FFTW: an adaptive software architecture for the FFT," in *Acoustics, Speech and Signal Processing, 1998. Proceedings of the 1998 IEEE International Conference on*, vol. 3, May 1998, pp. 1381–1384 vol.3.

[80] "Fast Fourier transform, MATLAB documentation," https://se.mathworks.com/help/matlab/ref/fft.html, accessed: 2016-12-21.

[81] P. J. D. Gething, *Radio Direction Finding and Superresolution*. Norwood, MA: P. Peregrinus, 1991.

[82] *Silicon Germanium 24 GHz Transceiver MMIC*, Infineon, July 2014, rev. 3.2.

[83] *Direct Modulation/Waveform Generating, 6.1 GHz Fractional-N Frequency Synthesizer*, Analog Devices, March 2014, rev. G.

[84] *32-bit Microcontrollers (up to 512 KB Flash and 128 KB SRAM) with Graphics Interface, USB, CAN, and Ethernet*, Microchip Technology, March 2013, rev. H.

[85] SICK, "Dx50-2: Mid range distance sensors," Brochure, July 2014, accessed: 2016-09-11.

[86] "Antenna and material measurements, VTT," http://www.vtt.fi/files/research/mel/antenna_and_material_measurements.pdf, accessed: 2016-02-11.

[87] S. M. Kay, *Funtamentals of Statistical Signal Processing: Estimation Theory.* Upper Saddle River, NJ: Prentice Hall, 1993.

[88] A. Chaudhari, S. Prabhu, and R. Pinto, "Frequency Estimator To Improve Short Range Accuracy in FMCW Radar," in *2015 International Conference on Advances in Computing, Communications and Informatics (ICACCI)*, 2015, pp. 640–644.

[89] E. Jacobsen and P. Kootsookos, "Fast, Accurate Frequency Estimators," *IEEE Signal Processing Magazine*, vol. 24, no. 3, pp. 123–125, 2007.